EGYPTIAN ACADEMIC JOURNAL OF
BIOLOGICAL SCIENCES
MICROBIOLOGY
G

ISSN
2090-0872
WWW.EAJBS.EG.NET
Vol. 16 No. 2 (2024)

Citation: *Egypt. Acad. J. Biolog. Sci. (G. Microbiolog) Vol.16 (2) pp.11- 47 (2024)*
DOI: 10.21608/EAJBSG.2024.371561

Egypt. Acad. J. Biolog. Sci., 16(2):11-47 (2024)

Egyptian Academic Journal of Biological Sciences
G. Microbiology

ISSN: 2090-0872
https://eajbsg.journals.ekb.eg/

Multistep Mutagenesis and Molecular Docking Studies of *Aspergillus flavus* AFK3 Enhancing Keratinase Expression for Feather Degradation

Nagwa M. Abd El-Aziz[1], Bigad E. Khalil[1]; Nora N. El-Gamal[2] and Hayam F. Ibrahim[3]

[1]Microbial Genetic Department, Biotechnology Research Institute, National Research Centre, 33 El Buhouth ST, Postal code 12622, Dokki, Cairo, Egypt.

[2]Microbial Chemistry Department, Biotechnology Research Institute, National Research Centre, 33 El Buhouth ST, Postal code 12622, Dokki, Cairo, Egypt.

[3]Genetics and Cytology Department, Biotechnology Research Institute, National Research Centre, 33 El Buhouth ST, Postal code 12622, Dokki, Cairo, Egypt.

*E.Mail: nagwamkh@gmail.com

ARTICLE INFO

Article History
Received:26/6/2024
Accepted:3/8//2024
Available:7/8/2024

***Keywords*:**
Keratinase, mutagenesis, ISSR-PCR, subtilisin, molecular docking.

ABSTRACT

In this study, we examined keratinase activity in twelve fungal isolates from various poultry markets, with isolate No.3 displaying the highest activity at 62.15 U/ml. Molecular analysis confirmed isolate 3 as *Aspergillus flavus* AFK3, a sequence deposited in the NCBI database. Sequential mutagenesis, involving ultraviolet (UV) radiation, ethyl methane sulfonate (EMS), and sodium azide (SA), led to the creation of the UV-33 mutant strain, which showed the most robust keratinase activity at 115.7 U/ml. Through Response Surface Methodology (RSM), we perfected culture conditions for the UV-33 mutant, achieving the highest keratinase activity at 133.73 U/ml under specific conditions of 1.5% malt extract, 1.5% fructose, pH 7, and 72 hours of incubation. A genetic diversity analysis compared *A. flavus* strain AFK3 with three mutants using inter-simple sequence repeat polymerase chain reaction (ISSR-PCR). The wild type AFK3 displayed the lowest band counts (28 bands with nonunique), while mutants UV-17, UV-33, and UV-24 had higher total and polymorphic bands, with UV-33 and UV-24 having 40 and 36 bands, respectively. Based on conserved regions, both *A. flavus* AFK3 and mutant *A. flavus* UV-33 were found to encode the *subtilisin* gene (*SUB*). The gene had an open reading frame of 2055 bp, which encoded a protein consisting of 684 amino acids. The 3D structure model was validated using Ramachandran's plot, indicating that residues were in the most favoured region and molecular docking studies revealed interactions with high-affinity scores for the template *A. flavus* strain CA14, wild type *A. flavus* AFK3, and mutant *A. flavus* UV-33 subtilisin, respectively.

INTRODUCTION

Keratins serve as integral constituents in various biological structures, such as wool, hooves, horns, hair, nails, and feathers. Notably, the USA, Brazil, and China collectively generate a staggering annual surplus of approximately 40 million tons of keratinous waste.

This waste originates from diverse sources, with a significant contribution from the global meat industry, particularly from slaughterhouses, which annually yield millions of tons of keratinous waste. For instance, chicken feathers alone account for up to two million tons of this waste **(**Reddy *et al*., 2021). The barbershop and fur business are two other places where keratinous waste is being produced. The sad truth is that now, only a small percentage of this waste—mainly from slaughterhouses being turned into animal feed. Because of its insolubility, keratins are mostly found on the bony surfaces of vertebrates. The existence of many disulfide bonds and strong stabilization of the polypeptide chains in these materials give them their structural stability. **(**Hassan *et al*., 2020).

In contrast to traditional protein-degrading enzymes such as pepsin and papain, keratins exhibit a remarkable resistance to degradation. Effective management of keratinous waste is of paramount importance, particularly in developing countries where the need for cost-effective solutions is pressing. Encouragingly, a promising avenue has emerged through the use of fungi and bacteria capable of producing extracellular keratinolytic enzymes, known as keratinases **(**Gafar *et al*., 2020). Keratinophilic fungi, adept at breaking down keratinaceous materials, are commonly found in diverse environments, spanning from soils in Antarctica to tropical regions, as well as in agricultural soils **(**Gunyar *et al*., 2020). These microorganisms are known to secrete keratinases, which are inducible extracellular enzymes. Various fungal genera, including *Aspergillus*, *Chrysosporium*, *Trichophyton*, and *Microsporum*, have been identified as keratinase producers **(**Akram *et al*., 2020).

Protease enzymes, including keratinases, have diverse applications across industries. Commercial keratinase powder, derived from *Bacillus licheniformis* and *Parengyodontium* album, finds use in pharmaceuticals for vaccine production, bioactive peptide preparation, and skin care products (Bohacz *et al*., 2020). It is also employed in cosmetic formulations like anti-dandruff shampoos and nutritional lotions. In industries such as feed production, nitrogen fertilizers, and leather, keratinases are used (Moridshahi *et al*., 2020). Additionally, they offer a sustainable solution for treating keratin-rich wastewater (Vidmar and Vodovnik 2018). Several keratinolytic fungi, including *Acremonium*, *Aphanoascus*, *Aspergillus*, and others, have been identified, with many being pathogenic (Abirami *et al*., 2020). Non-pathogenic strains are preferable for industrial use, necessitating further research for suitable microorganisms. Keratinases exhibit broad temperature (40–70°C) and pH (6–11) ranges, emphasizing the importance of optimizing conditions for their industrial applications (Bagewadi *et al*., 2018).

Fungal keratinases are proteases that efficiently break down tough keratin, making them valuable for various applications. They are particularly attractive due to their ability to act on a wide range of insoluble keratin substrates. Fungal keratinases, produced extracellularly or intracellularly by fungi like dermatophytes and saprotrophic ascomycetes, offer a cost-effective and efficient method for processing keratin waste. Enzymes like these have a wide range of uses, including inducible hair removal from skin and hide, textile processing, detergent formulation, medicines, cosmetics, and the creation of bioactive peptides. Microbial decomposition of keratinous waste is more efficient, produces useful hydrolysates for feed, agriculture, and food production, and is more selective than chemical treatments. Fungal keratinases are highly productive due to the filamentous growth of their producers, making them a valuable

resource for industrial and environmental applications. (Bhari and Kaur 2023).

Keratinase enzymatically breaks down keratin, a protein that serves as a protective barrier. It possesses a high degree of rigidity, is resistant to change or control, and cannot be broken down by other enzymes that break down proteins. The active site determines whether a keratinase is a serine protease, a metalloprotease, or a metalloprotease. A subset of keratinases, known as serine proteases, have an active serine core and are hence members of the subtilisin-like protease superfamily (S8 family). **(**Gurunathan *et al*., 2021).

The objective of this research was to identify a fungal strain with elevated keratinase production, followed by enhancing its keratinase activity through mutagenesis and molecular docking studies. This approach leveraged genetic diversity and explored subtilisin, promising applications in the field of biotechnology. The study's comprehensive approach aimed to harness the potential of these enzymes for various biotechnological applications.

MATERIALS AND METHODS

Collecting Samples:

Ten different poultry waste samples were collected from ten different local poultry markets with permission to collect samples in sterile containers from Cairo City, Egypt.

Microorganisms and Culture Conditions:

The feather meal basal medium (FMBM), as described in (El-Ghonemy and Ali 2017) had the following composition (g/L): KH_2PO_4, 1.0; $MgSO_4 \cdot 7H_2O$, 0.5; KCl, 0.5 and adjusted to pH 6.0. containing 10 gm of chicken feathers, served as the primary medium for isolating and fermenting the feather-degrading fungi. Fungal preparations were carried out using malt extract (ME) agar medium (Himedia, West Chester, Pennsylvania, USA). The fungal strain *A. flavus* AFK3, known for its keratinolytic activity, was isolated based on colony morphology on FMBM agar plate medium containing 10 g/l of a white chicken feather, thus; it was further identified as a keratinase-producing fungus. A single colony was chosen and inoculated onto an ME agar slant, which was then incubated at 28°C for three days. Subsequently, the slant was stored at 4°C for future investigations. Using the procedure outlined, soluble keratin was produced using chicken feathers collected from local poultry waste (El-Ghonemy and Ali 2017).

Preparation of Crude Enzyme Extract and Keratinase Enzyme Assay:

A single, pure colony of the chosen fungal isolate that had been grown on ME agar medium was transferred under sterile conditions to produce keratinase using the fermentation feather meal basal (FMBM) medium, following the procedure outlined in (El-Ghonemy and Ali 2017). A quantitative keratinase test was performed on the supernatant that was collected after incubation, which included the released enzyme. The substrate used to test the activity of the keratinase enzyme was a keratin solution. To determine the keratinase activity, refer to the procedure described in (El-Ghonemy and Ali 2017; Gradisar *et al*., 2005), In a 0.1 M Tris-acetate buffer (pH 8.0), 1 ml of keratin and 1.0 ml of cell-free supernatant (crude enzyme) were incubated for 10 minutes. A rise in the adjusted absorbance at 280 nm (A_{280}) relative to the control group (the identical treatment group that did not receive a keratin solution) at a rate of 0.01 per minute under the given experimental conditions was one unit (U/ml) of keratinolytic activity. $U = 4 \times n \times A_{280} / (0.01 \times 10)$, where n was the dilution rate, 4 was the final reaction volume in milliliters, and 10 was the incubation period in minutes, which was the formula used to determine the activity.

Determination of Protein Content and Residual Hydrolysates:

Protein content was assessed following the procedure outlined in (Bradford 1976), as the gold standard is

bovine serum albumin. The leftover hydrolysates were feathers and cells that had not been digested. The procedure described was used to ascertain the mass of these remaining hydrolysates. (Cai *et al*., 2008).

Molecular Identification of Keratinolytic Fungi:

DNA extraction was performed using the extraction method provided by Applied Biotechnology Co., Egypt. To identify the fungal isolate, we partially sequenced the ITS region using universal primers. The forward primer ITS1 (5'-TCC GTA GGT GAA CCT GCG G-3') and reverse primer ITS4 (5'-TCC TCC GCT TAT TGA TAT GC-3') were used. The PCR product was purified, labeled, and sequenced following the protocols outlined (White *et al*., 1990). We ran the polymerase chain reaction (PCR) at 95°C for 3 minutes to denature the DNA, then we cycled through 35 cycles of denaturation, annealing, and extension at 72°C for 30 and 55°C, respectively. The procedure ended with a 5-minute extension at 72°C. The Mega Quick-Spin total fragment DNA purification kit was used to purify the PCR product according to the manufacturer's instructions. The Sanger technique was used to conduct the sequencing. The acquired sequence was subjected to BLAST searches using the "blastn" programme provided at NCBI (www.ncbi.nlm.nih.gov/BLAST) to determine the likely strain identification. According to the BLAST findings, the strain was identified as *A. flavus* with the accession number OK086056, based on sequence homology. Following the steps outlined in, we used MAFFT alignment to build a phylogenetic tree. **(**Rozewicki *et al*., 2019). The alignment was conducted using the MAFFT alignment server for phylogeny (https://mafft.cbrc.jp/alignment/server/phylogeny.html).

Ultraviolet (UV) Radiation, Ethyl Methane Sulfonate (EMS), and Sodium Azide (SA) Mutagenesis:

Cultures of the organism's native form, *A. flavus* AFK3, were incubated in an ME broth medium at 30°C for 2–5 days. Following that, the cellular biomass was separated by centrifugation of a 10-millilitre sample of the culture at 9000g and 4°C for 10 minutes. After that, 10 millilitres of sterile saline solution with a salt content of 0.9% was added to the cellular biomass pellet. This preparation was used for ultraviolet UV-induced mutagenesis. (Magda and Sanaa 2018), For this experiment, we used a UV dispensing cabinet to expose four millilitres of culture per sterile petri dish to ultraviolet radiation. Almost 90% of the energy released by the 15-W bulbs in the cabinet was at a wavelength of 265 nm. After being treated to UV radiation for 60 minutes, the plates were put 30 cm away from the center of the source. Subsequently, the plates that had been treated were placed in a dark environment and left to incubate overnight to avoid photoreactivation. To initiate mutagenesis, ethyl methane sulfonate (EMS) and sodium azide (SA) might be employed (Akbar *et al*., 2013; Akbar *et al*., 2015; Kamalambigeswari *et al*., 2018), separate plates were supplemented with a 3% (v/v) aqueous EMS solution and 0.1% sodium azide. The plates were thereafter placed in an incubator set at a temperature of 30°C for a duration of 60 minutes. After all mutagenesis treatments, the cells were collected by spinning them with a force of 2800 times the acceleration due to gravity for a duration of 15 minutes. Then, the cells were rinsed with a sterile solution of salt. Consecutive dilutions were made, and then a 0.1 ml portion of the mixture was evenly distributed on ME agar plates. The plates were subjected to incubation at a temperature of 30°C for a duration ranging from 2 to 5 days. The colonies of *A. flavus* AFK3 that emerged were assessed for their keratinase activity to identify mutants that produce keratinase with high efficiency, as outlined in **(**Duarte *et al*., 2011).

Optimization of Keratinase Activity Using the Response Surface Methodology:

A two-step statistical design approach was used to optimize keratinase production by the mutant *A. flavus* UV-33. The experimental design and statistical analysis were carried out using the Design-Expert® 6.0.8 statistical software (Stat-Ease, Minneapolis, MN, USA) (Barman *et al.*, 2017; Gupta and Singh 2013). This process began with the identification of potential carbon and nitrogen sources for keratinase by screening them. The following carbon and nitrogen sources were examined at a concentration of 0.5%: glucose, sucrose, fructose, lactose, and xylose; peptone, tryptone, malt extract, beef extract, and yeast extract. Step two of the research process included using Response Surface Methodology (RSM), by the Plackett-Burman design shown in Table 1. This stage assessed the impact of various factors at two distinct values, including pH levels (5, 6, 7, 8, and 9), incubation duration (1, 2, and 3 days), carbon source (fructose), and nitrogen source (malt extract). RSM is a two-factor experimental design with three levels for each factor (Saxena and Singh 2010). A total of 30 experimental designs were conducted, and keratinase activity was measured as the response variable. The keratinase activity data obtained from the experiments were analyzed using the general model equation: $Y = \beta o + \beta 1X1 + \beta 2X2 + \beta 3X3 + \beta 11X12 + \beta 22X22 + \beta 33X32 + \beta 12X1X2 + \beta 13X1X3 + \beta 23X2X3$. We used Fisher's F test and analysis of variances ($p < 0.05$) to find out how significant each coefficient in the equation was. 3D contour plots were used to represent the quadratic models **(**Tiwary and Gupta 2010). Furthermore, the keratinase production data obtained from RSM were subjected to analysis of variance (ANOVA). All experiments were conducted in triplicate.

Table 1: The Plackett-Burman factorial design (PBFD) was used for statistical screening, together with the experimental components and levels of minimum and maximum range.

Factors	Independent Factor	Unit	Type	Range Level		
				Minimum (−1)	Medium (0)	Maximum (+1)
X1	Incubation time	Hours	Factor	24	48	72
X2	pH	+H	Factor	5	7	9
X3	Fructose (carbon source)	% (w/v)	Factor	0.5	1.5	2.5
X4	Malt extract (nitrogen source)	% (w/v)	Factor	0.5	1.5	2.5
X5	Keratinase activity	U/ml	Response			

Molecular Markers ISSR-PCR for Fungal Wild-Type and Mutant Strains:

Molecular genetics played a significant and effective role in identifying genetic variations among different genotypes, forming the basis for the isolation of *A. flavus* AFK3 (accession number OK086056) and its mutants (UV-33, UV-24, and UV-17) at the molecular level. To analyze these genetic differences, we conducted inter-simple sequence repeat (ISSR) analysis following the procedure outlined in **(**Zietkiewicz *et al.*, 1994) together with materials sourced from UBC's biotechnology lab in Vancouver, Canada. As shown in Table 2, the study's ISSR primers focused on core repeats that were anchored at either the 5' or 3' ends. Using the Ama Rone PCR master mix and Taq DNA polymerase chain reaction (PCR), the DNA samples from the four fungal genotypes were amplified following the manufacturer-provided directions. The first step of the PCR reaction was a 5-minute incubation period at 94°C. After that, there were forty steps of denaturation

at 94°C for fifty seconds, annealing at 45°C for one minute, and extension at 72°C for one minute. Finally, an elongation stage was run for 10 minutes at 72°C. Following amplification, the PCR products were electrophoretically separated into a 1.5% agarose gel. Electrophoresis was carried out using a TAE buffer and a red-safe dye concentration of 0.004%. To determine the molecular weight of each band and to compare the presence or absence of bands across various cultivars, the gel was photographed using gel documentation (Bio-Rad) and evaluated using the Total Lab software. To generate the similarity matrix and dendrogram, the data was imported into the statistical program MVSP Version 3.1.

Table 2: the ISSR primer name and sequences

Primers	Sequence	Annealing temperature
ISSR-152	5'- (AG)8YC-3'	45ºC
UBC 851	5'- (GT)8YG-3'	
ISSR -157	5'- CGCGATAGATAGATAGATA-3'	
ISSR- 158	5'- GACGATAGATAGATAGATA-3'	
ISSR-861	5'- (GT)6YG-3'	

Subtilisin Encoding Gene Amplification:

Firstly, the primers for the *SUB*-encoding gene of *A. flavus* strain CA14 were designed using its DNA sequence. Genomic DNA was extracted from the *A. flavus* AFK3 (NCBI Accession No. OK086056) and mutant *A. flavus* UV-33 using a genomic DNA isolation kit and used as a template for amplifying the *SUB* gene. Then, the *SUB* encoding gene was amplified from *A. flavus* AFK3 and mutant *A. flavus* UV-33 using specific primers as follows: forward primer *SUB*-F (*5′*-ATGTCTGTTATTACCATTAATGGCA ATTC-3′), and the reverse primer was *SUB*-R (*5′*-TTAAGTAAGTCGCCAG GC GC-3′), Obtained using Primer3 software, the SUB gene sequence was determined. The DNA sequence of the SUB gene, which consists of 2055 nucleotides and codes for a protein with 684 amino acids, was used as a template for amplifying the SUB gene sequence by polymerase chain reaction (PCR). **(**Banerjee *et al*., 2014). The manufacturer's instructions were followed throughout the testing procedures. The 100 µl reaction, which included 5 µM primers and 100 ng of genomic DNA, was carried out using a Gene Amp PCR System 2400 thermal cycler from PerkinElmer in Norwalk, Connecticut, USA. The master mix was sourced from TIANGEN in Beijing, China. The 35-cycle PCR technique began with a 5-minute denaturation phase at 95°C, then 1 minute of denaturation at 95°C, 1 minute of annealing at 55°C, and 2 minutes of extension at 72°C for each kilobase pair (kbp). The last element of the programme was an extension at 72°C for three minutes. **(**Gupta *et al*., 2017). Using the FavorPrep GEL Purification kit (FAVORGEN, Biotech Corp., Ping Tung, Taiwan), the 2055 bp band encoding the SUB gene was extracted from the 1% agarose gel after the PCR products were analysed on the gel. After isolating the band, it was submitted for sequencing after being purified using the Qiagen gel purification kit.

Bioinformatics Analysis:

The experimentally determined subtilisin gene sequences of *A. flavus* AFK3 and mutant *A. flavus* UV-33 were translated into protein sequences using the online translation tool ExPASY (http://web.expasy.org/translate). The *subtilisin* sequence was characterized by conducting searches in the GenBank nucleotide and amino acid sequence databases at the National Centre for Biotechnology Information (NCBI) server using BLASTN and BLASTP algorithms

(http://blast.ncbi.nlm.nih.gov/Blast.cgi).
The open reading frame of the *subtilisin* gene was analyzed using the "Open Reading Frame Finder" tool available on the NCBI website (ORFfinder Viewer, NCBI (nih.gov)).To further scrutinize the protein sequences, a multiple sequence alignment (MSA) was carried out using the PRALINE online resource portal (http://www.ibi.vu.nl/programs/pralinewww/). This alignment facilitated the comparison and alignment of multiple protein sequences to detect conserved regions and similarities. Additional information on the utilization of PRALINE for sequence alignment can be found in the studies by **(**Liu *et al.*, 2013; Eramian *et al*., 2006). Secondary structure prediction of the *subtilisin* protein was carried out using the online PDBsum server PDBsum home page (ebi.ac.uk). Cluster analysis (phylogenetic tree) of the *A.flavus* subtilisin protein sequence was carried out using the MEGAX software (megax-software [ILRI Research Computing] (cgiar.org)).

Homology Modelling, Validation, and Binding Pockets Prediction of *subtilisin:*

To predict the tertiary structure of *subtilisin* protein, I-TASSER (http://I-TASSER server for protein structure and function prediction (zhanggroup.org) was used (Banerjee *et al*., 2014; Yang and Yang 2015). Out of the five models created the model with the highest confidence score (C-score) and potential energy was chosen for future investigation. (Sahi *et al.*, 2012; Singh and Muthusamy 2013). The C-score often falls within the range of -5 to 2. The C-score value and the structure quality have a direct correlation. The subtilisin protein's validation structure was confirmed using the SAVES v6.0 (structure analysis and verification server version 6) online program (http://SAVESv6.0 - Structure Validation Server (ucla.edu) and the ProSA server. SAVES v6.0 is a comprehensive suite of five applications designed to assess the overall coherence of a protein structure. We employed VERIFY-3D among five programs to assess the 3-D sequence profile of protein models, and PROCHECK to validate the structure using the Ramachandran plot. (Kulkarni and Devarumath 2014). Afterwards, the "subtilisin" software (DeLano Scientific LLC) was used to generate a stereo image of the subtilisin model, which clearly shows the surface groove structure. (Gupta *et al*., 2017). The Site-Map module of the deepsite/play molecule online tool (http://DeepSite: a binding pocket predictor using neural-networks [WEB APP] (playmolecule.com) was used for binding site predictions in the *subtilisin* protein and ligand beta keratin (Kesharwani and Misra 2011). To identify potential binding sites of amino acids, we considered physical characteristics such as size, degree of enclosure or exposure, hydrophobic or hydrophilic nature, tightness, and hydrogen-bonding potential. (Banerjee *et al*., 2014).

Molecular Docking Studies:

The MOE software (Molecular Operating Environment (MOE) | MOEsaic | PSILO (chemcomp.com) was employed to process the 3D structure of *subtilisin* by removing water molecules, ions, and existing ligands from the protein molecule. Subsequently, the insertion of hydrogen atoms into the receptor molecule was conducted using PyMOL software (PyMOL | pymol.org) (Banerjee *et al*., 2014; Sahi *et al*., 2012). The structure data format (PDB) of the substrate (beta keratin, PubChem CID: 395651, PF02422), which was downloaded, was processed using MOE and PyMOL software. The substrate molecule was then converted to a dockable PDB format using PyMOL software (Banerjee *et al*., 2014; Sahi *et al*., 2012). Docking studies were conducted to investigate the binding mode of beta-keratin as a substrate with the 3-D model of the *subtilisin* protein using the HDock online tool (http:// HDOCK Server (hust.edu.cn). The resulting macromolecule file was saved in PDB format for docking purposes. Gasteiger-type charges were assigned to polar H atoms, nonpolar H

atoms were combined with carbons and internal degrees of freedom and torsions were configured (Banerjee *et al*., 2014; Gupta *et al*., 2017; Sahi *et al*., 2012).

RESULTS

Isolation and Quantitative Keratinase Assays of Fungal Isolates:

Twelve fungal colonies were obtained from samples of poultry waste taken from 10 distinct local poultry markets in Cairo, Egypt. The fungal isolates were chosen based on their unique morphological traits and then stored on malt extract agar slants for future examination. The fungal strains that were kept apart from others were assessed to determine their ability to produce keratinase and their unique activities. The findings demonstrated a diverse spectrum of keratinase activity among the isolates. Isolate number 3 exhibited the greatest level of keratinase activity, with a recorded reading of 62.15 U/ml. In addition, an assay was performed to determine the activity of keratinase in all isolates. This was done by evaluating the protein content of the feathers that remained after the process, which was measured at A_{280} as previously described. Isolate number 3, when grown in a basic medium, showed the highest level of keratinase activity. It had a remaining featherweight of 170±0.038 mg and a protein content of 1.113 mg/ml. This isolate exhibited rapid and thorough destruction of feathers during a span of 48 hours when exposed to a substrate consisting of 1% feathers. Consequently, this particular isolate was assigned the designation AFK3.

Molecular Identification of Fungus AFK3 Using ITS Region Gene Alignment in GenBank (Blast) and Phylogenetic Tree Analysis:

The nucleotide sequence of the ITS region gene from the AFK3 isolate was submitted to GenBank with the accession number OK086056. To ascertain the likely identity of the strain, we subjected the obtained sequence to BLAST queries using the "blastn" algorithm on the NCBI website (www.ncbi.nlm.nih.gov/BLAST). Based on sequence homology, the top result from the BLAST analysis indicated that this nucleotide sequence shared 99% similarity with *Aspergillus flavus*. Consequently, the isolate was identified as *Aspergillus flavus*, specifically the AFK3 strain. The phylogenetic tree, constructed using the ITS region sequence, illustrated that the AFK3 isolate fell within the same group and exhibited a close relationship with *Aspergillus flavus*, as shown in Figure 1.

Fig. 1: phylogenetic tree of ITS regions of *Aspergillus flavus* AFK3 and the other strains in Genbank

***Aspergillus flavus AFK3* Multistep Mutation Induction for Keratinase Production Improvement:**

In the initial mutation step, the *Aspergillus flavus* AFK3 strain underwent ethyl methanesulfonate (EMS) mutagenesis to improve its keratinase production. Following exposure to EMS for 60 minutes, a total of fifty-nine surviving colonies of *Aspergillus flavus* AFK3 were isolated. These colonies were subsequently assessed for keratinase activity, and only four mutants demonstrated significantly enhanced keratinase activity. Among these mutants, EMS-40 exhibited the highest level of hyperactivity, recording a value of 74.93 U/ml. Furthermore, the residual featherweight for EMS-40 was determined to be 150±0.055 mg, with a protein content of 1.262 mg/ml. These values exceeded those of the wild-type strain *Aspergillus flavus* AFK3 (62.15 U/ml), as outlined in Table 3.

For the second phase of mutation, the EMS-40 mutant underwent treatment with 0.1% sodium azide (S.A.) mutagenesis for 60 minutes. Thirty-five surviving colonies were isolated and assessed for keratinase activity. Among these colonies, five mutants demonstrated significantly enhanced keratinase activity. The most hyperactive mutant among them was S.A-9, recording a value of 98.60 U/ml. The residual featherweight for S.A-9 was determined to be 110±0.098 mg, with a protein content of 1.350 mg/ml. However, these values were lower than those of the wild-type mutant EMS-40 (74.93 U/ml).

In the third mutation step, the S.A-9 mutant underwent ultraviolet (UV) mutagenesis for 60 minutes. After the treatment, thirty-eight surviving colonies were isolated and evaluated for keratinase activity. Among these colonies, only three mutants displayed improved efficiency in keratinase activity. The most hyperactive mutant among them was UV-33, which achieved a value of 115.44 U/ml. The residual featherweight for UV-33 was determined to be 80±0.068 mg, with a protein content of 1.395 mg/mL. These values exceeded those of the wild-type mutant S.A-9 (98.60 U/ml), as detailed in Table 3.

Table 3: Estimation of keratinase activity produced by mutants and parent strain *Aspergillus flavusAFK3 after* three days incubation at 28^{o}C.

***Aspergillu sflavus* AFK3strain**	**Keratinase activity (U/ml)**	**Residual feather (mg)**	**Protein content (mg/ml)**
First step mutation with ethyl Metha sulfonate (EMS)*mutagenesis			
Parent *A. flavus*AFK3strain	**62.15**	**170±0.036**	**1.113**
EMS-Mutants			
EMS-12	69.22	160±0.074	**1.233**
EMS-40	**74.93**	**150±0.055**	**1.262**
EMS-43	67.21	160±0.024	**1.242**
EMS-51	65.98	170±0.012	**1.257**
Second step mutation with sodium azide (S.A) ** mutagenesis			
Parent E-40	**74.93**	**150±0.055**	**1.262**
S.A-mutants			
S.A-9	**98.60**	**110±0.098**	**1.350**
S.A-18	79.90	140±0.040	**1.315**
S.A-24	87.67	120±0.033	**1.173**
S.A-31	82.38	120±0.084	**1.267**
S.A-35	76.45	150±0.083	**1.256**
Third step mutation with ultraviolet (UV)mutagenesis			
Parent S.A-9	**98.60**	**110±0.098**	**1.350**
UV-mutants			
UV-17	95.78	100± 0.031	**1.234**
UV-24	98.80	90±0.013	**1.264**
UV-33	**115.7**	**80± 0.068**	**1.395**

*EMS: 3%concentration** S.A:0.1% concentration

Screening of Significant Carbon and Nitrogen Variables:

The mutant *A. flavus* UV-33 mutant exhibited a noteworthy influence of 10 carbon and nitrogen supply factors on keratinase production. This influence was quantified by the E(xi) value, which ranked the variables under investigation. A coefficient close to zero signified minimal or no effect, whereas a high positive or negative E(xi) coefficient indicated a substantial impact on the response. Except for malt extract (89.27 U/ml) and fructose (92.35 U/ml) additions, all other variables had a positive effect on keratinase production, as detailed in Figures 2a and b.

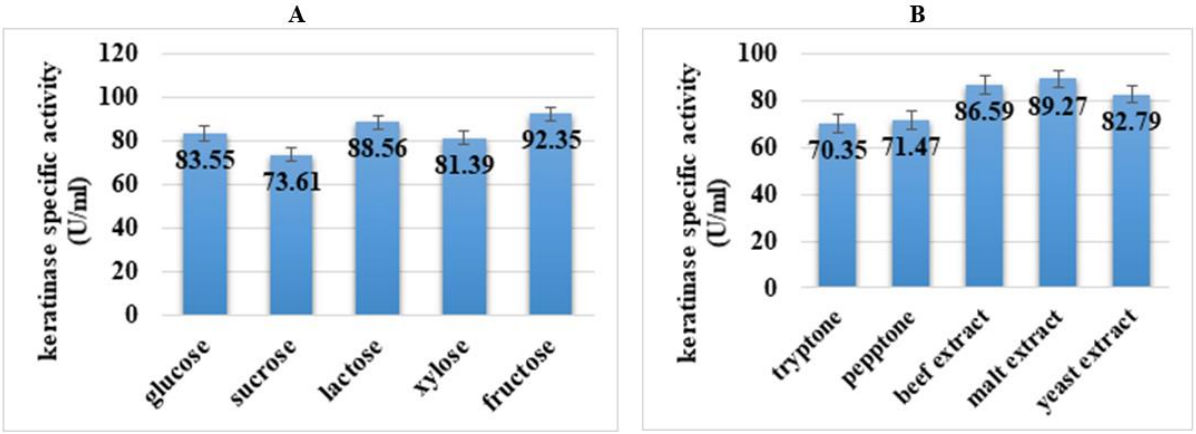

Fig. 2: Medium optimization conditions by supplementing different **A**; carbon sources. **B**; nitrogen sources of mutant UV-33

Optimization of Keratinase Activity Using Response Surface Methodology:

Using response surface methodology (RSM), the optimal concentration of medium components and incubation duration was determined by selecting four variables: fructose, malt extract, pH, and incubation time. Tables 4 and 5, presented the design matrix, RSM trial results, mean predicted values and residual values to assess the effects of these independent variables. The experiment comprised a 30-trial matrix with three levels (-1, 0, and +1) for each of the four components, along with three repetitions at the central point. The highest keratinase production, reaching 133.73 U/ml, was achieved with 1.5% malt extract, 1.5% fructose, pH 7, and 72 hours of incubation. The analysis of variance for the quadratic regression model indicated its high significance (F-value of 21.76) (Table 4). The adjusted determination coefficient (Adj R-Squared) reached 0.9009, which was supported by the Adeq precision measure signifying a high signal-to-noise ratio. This resulted in a predictive R-squared value of 0.9487, indicating a strong correlation as per the F-test (Tables 6 and 7). The R-squared value denotes the proportion of variability in the observed response values that can be accounted for by the experimental factors and their interactions. To scrutinize the effects and variable responses, response surface plots were generated, displaying pairwise combinations of the three factors while holding one at its optimal level: as shown in Figure 3.

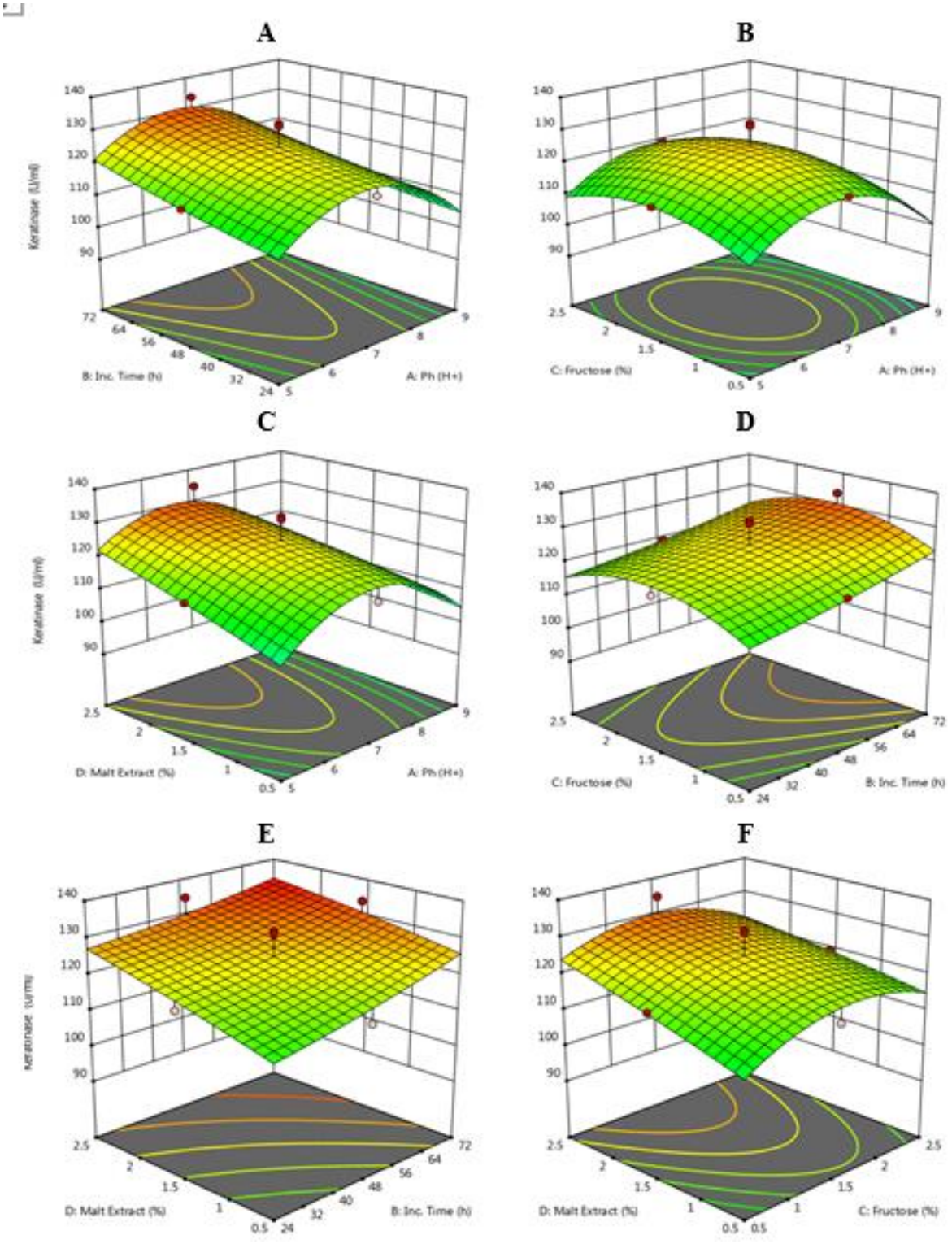

Fig 3: Contour plots were generated to analyze the enzyme activity of mutant A. flavus UV-33. The plots focused on the interactions between four variables: (**A**) incubation time and pH, (**B**) fructose% and pH, (**C**) malt extract % and pH, and (**D**) fructose % and incubation time. Additionally, the plots examined the interactions between (**E**) malt extract % and incubation time, and (**F**) malt extract % and fructose %. These plots provide valuable insights into the impact of these variables on keratinase production.

Adequacy of the Model:

The model's validity was confirmed through experimental reevaluation, which entailed testing keratinase production using a random selection of 30 production combinations. According to the ultimate optimized conditions, the projected keratinase production response was 133.73 U/ml, while the observed experimental value stood at 130.82 U/ml, as documented in Table 4. The experimental results closely matched the expected values, thus affirming the model's validity.

Table 4: Design of different trials of the response surface methodology for independent variables and responses by fungal mutant *A. flavus* UV-33

Run	Factor 1 A: ph H+	Factor 2 B: Inc. time h	Factor 3 C: fructose %	Factor 4 D: malt Extract %	Actual value keratinase U/ml	Predicted Value	Residual
1	7(0)	48(0)	1.5(0)	1.5(0)	121.26	124.82	**-3.57**
2	9(+1)	24(-1)	2.5(+1)	0.5(-1)	97.71	96.45	**1.26**
3	5(-1)	24(-1)	2.5(+1)	2.5(+1)	111.70	111.13	**0.5708**
4	5(-1)	72(+1)	0.5(-1)	0.5(-1)	105.43	104.89	**0.5381**
5	5(-1)	24(-1)	0.5(-1)	0.5(-1)	90.39	90.10	**0.2908**
6	9(+1)	24(-1)	2.5(+1)	2.5(+1)	100.69	101.29	**-0.5952**
7	7(0)	48(0)	1.5(0)	1.5(0)	121.98	124.82	**-2.84**
8	7(0)	48(0)	1.5(0)	1.5(0)	120.95	124.82	**-3.87**
9	7(0)	24(-1)	1.5(0)	1.5(0)	118.40	121.16	**-2.76**
10	9(+1)	72(+1)	2.5(+1)	0.5(-1)	105.17	105.68	**-0.5090**
11	7(0)	48(0)	1.5(0)	1.5(0)	131.25	124.82	**6.43**
12	5(-1)	24(-1)	2.5(+1)	0.5(-1)	96.70	96.50	**0.2077**
13	9(+1)	72(+1)	0.5(-1)	2.5(+1)	108.12	108.39	**-0.2647**
14	9(+1)	72(+1)	2.5(+1)	2.5(+1)	105.54	105.81	**-0.2719**
15	7(0)	72(+1)	1.5(0)	1.5(0)	133.73	130.82	**2.91**
16	9(+1)	24(-1)	0.5(-1)	0.5(-1)	92.23	91.06	**1.17**
17	7(0)	48(0)	1.5(0)	1.5(0)	120.99	124.82	**-3.83**
18	5(-1)	72(+1)	2.5(+1)	2.5(+1)	118.41	119.64	**-1.22**
19	5(-1)	72(+1)	2.5(+1)	0.5(-1)	110.32	109.71	**0.6130**
20	7(0)	48(0)	1.5(0)	2.5(+1)	131.70	128.53	**3.17**
21	9(+1)	72(+1)	0.5(-1)	0.5(-1)	101.32	101.87	**-0.5519**
22	9(+1)	24(-1)	0.5(-1)	2.5(+1)	101.69	102.29	**-0.5941**
23	9(+1)	48(0)	1.5(0)	1.5(0)	108.70	108.35	**0.3562**
24	7(0)	48(0)	2.5(+1)	1.5(0)	119.40	119.45	**-0.0553**
25	7(0)	48(0)	0.5(-1)	1.5(0)	117.75	117.54	**0.2078**
26	5(-1)	48(0)	1.5(0)	1.5(0)	114.58	114.78	**-0.2038**
27	7(0)	48(0)	1.5(0)	0.5(-1)	114.93	117.95	**-3.02**
28	5(-1)	72(+1)	0.5(-1)	2.5(+1)	119.96	121.20	**-1.24**
29	7(0)	48(0)	1.5(0)	1.5(0)	132.05	124.82	**7.23**
30	5(-1)	24(-1)	0.5(-1)	2.5(+1)	111.58	111.12	**0.4519**

Table 5: Analysis of variance table (ANOVA for Response Surface Quadratic Model CCD) by fungal mutant *A. flavus* UV-33

Source	Sum of Squares	Df	Mean Square	F-value	p-value	
Model	3823.56	14	273.11	21.76	< 0.0001	significant
A-Ph	186.17	1	186.17	14.83	0.0016	
B-Inc. Time	419.63	1	419.63	33.43	< 0.0001	
C-Fructose	16.40	1	16.40	1.31	0.2709	
D-Malt Extract	503.42	1	503.42	40.10	< 0.0001	
AB	15.82	1	15.82	1.26	0.2792	
AC	1.02	1	1.02	0.0809	0.7799	
AD	96.00	1	96.00	7.65	0.0144	
BC	2.49	1	2.49	0.1984	0.6624	
BD	22.17	1	22.17	1.77	0.2038	
CD	40.78	1	40.78	3.25	0.0916	
A^2	455.44	1	455.44	36.28	< 0.0001	
B^2	3.51	1	3.51	0.2799	0.6045	
C^2	103.66	1	103.66	8.26	0.0116	
D^2	6.49	1	6.49	0.5168	0.4833	
Residual	188.30	15	12.55			
Lack of Fit	44.30	10	4.43	0.1538	0.9939	not significant
Pure Error	144.00	5	28.80			

Factor Coding Is Coded:
The Sum of Squares Is Type III – Partial:

The Model F-value, which was 21.76, demonstrated the statistical significance of the model. The probability of obtaining such a substantial F-value by random chance alone was only 0.01%, indicating that the model's effects were not the result of random variability.

P-values below 0.0500 indicated the significance of the model terms. In this instance, terms A, B, D, AD, A^2, and C^2 were deemed significant. Conversely, model terms with p-values exceeding 0.1000 were considered not significant. If there were numerous insignificant model terms (excluding those essential for hierarchy), simplifying the model might enhance its performance.

The Lack of Fit F-value, at 0.15, indicated that the Lack of Fit wasn't statistically significant when compared to pure error. There was a 99.39% probability that such a Lack of Fit F-value could arise due to random variability. A non-significant lack of fit was favourable because it suggested that the model was a good fit for the data.

Table 6: Regression values by CCD

Std. Dev.	**3.76**	**R^2**	**0.9487**
Mean	112.92	**Adjusted R^2**	0.9009
C.V. %	3.33	**Predicted R^2**	0.8825
		Adeq Precision	15.2906

The Predicted R^2 of 0.8825 is in reasonable agreement with the Adjusted R^2 of 0.9009; i.e., the difference is less than 0.2.

Adeq Precision measures the signal-to-noise ratio. A ratio greater than 4 is desirable. Your ratio of 15.291 indicates an adequate signal. This model can be used to navigate the design space.

Table 7: Sequential model sum of squares

Source	Sum of Squares	Df	Mean Square	F-value	p-value	
Mean vs Total	3.819E+05	1	3.819E+05			
Linear vs Mean	1125.62	4	281.40	2.44	0.0735	
2FI vs Linear	178.28	6	29.71	0.2085	0.9697	
Quadratic vs 2FI	**2519.66**	**4**	**629.92**	**50.18**	**< 0.0001**	**Suggested**
Cubic vs Quadratic	44.21	8	5.53	0.2685	0.9574	Aliased
Residual	144.09	7	20.58			
Total	3.859E+05	30	12862.35			

Molecular Markers ISSR-PCR for Wild-Type and Mutant Fungal Strains:

In the molecular analysis conducted using ISSR-PCR primers, a total of 52 markers were generated through the application of five ISSR primers, specifically ISSR-152, UBC-851, ISSR-157, ISSR-158, and ISSR-861. Among these markers, 35 bands were identified as polymorphic, indicating a polymorphism rate of 63%. You can find this data in Table 8 and Fig. 4a. When it comes to the total number of bands, the mutant UV. -33 exhibited the highest count, with 40 bands, followed by the mutant UV. -24 with 36 bands and the mutant UV. -17 with 33 bands. In contrast, the wild-type strain AFK3 had the lowest total number of bands, recording only 28 bands in each category when compared to the mutants. These details are available in Table 9 and Fig. 4b. Furthermore, if we consider the number of polymorphic bands with unique patterns, UV-33, UV-24, and UV-17 displayed 23, 19, and 16 bands, respectively. On the other hand, strain AFK3 exhibited the lowest number of polymorphic bands with unique patterns, totalling 11 bands. This comparison is presented in Table 10 and Fig. 5. Throughout the ISSR analysis, various variations in the nucleotide sequence of the selected mutant DNA were detected and documented when compared to the wild-type strain *Aspergillus flavus* AFK3.

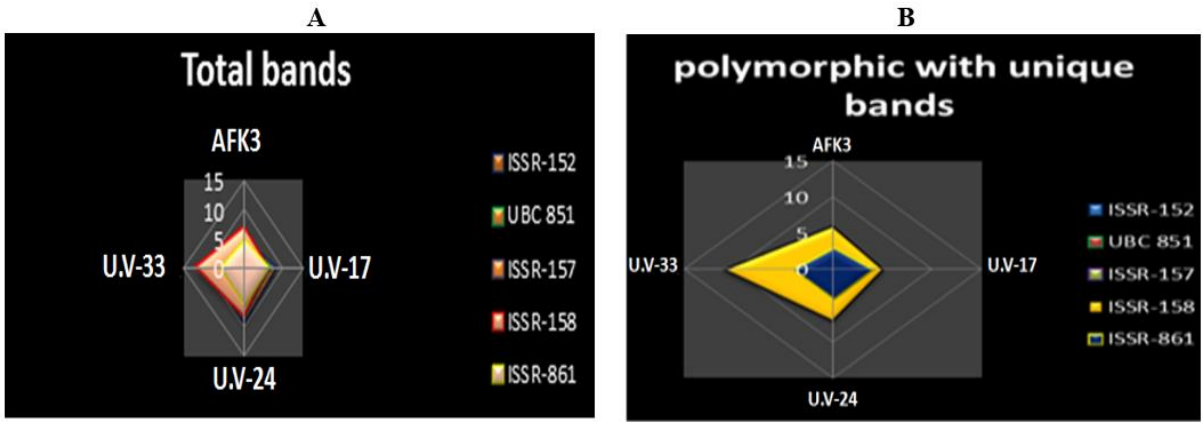

Fig. 4: A; the relationship between total bands of the different primers used for the detection of four samples of the strain, **B**: The relationship between, polymorphic with unique bands and polymorphism percentage of eight ISSR primers used for the detection of four fungi samples of strain *Aspergillus flavus* AFK3 and three mutants.

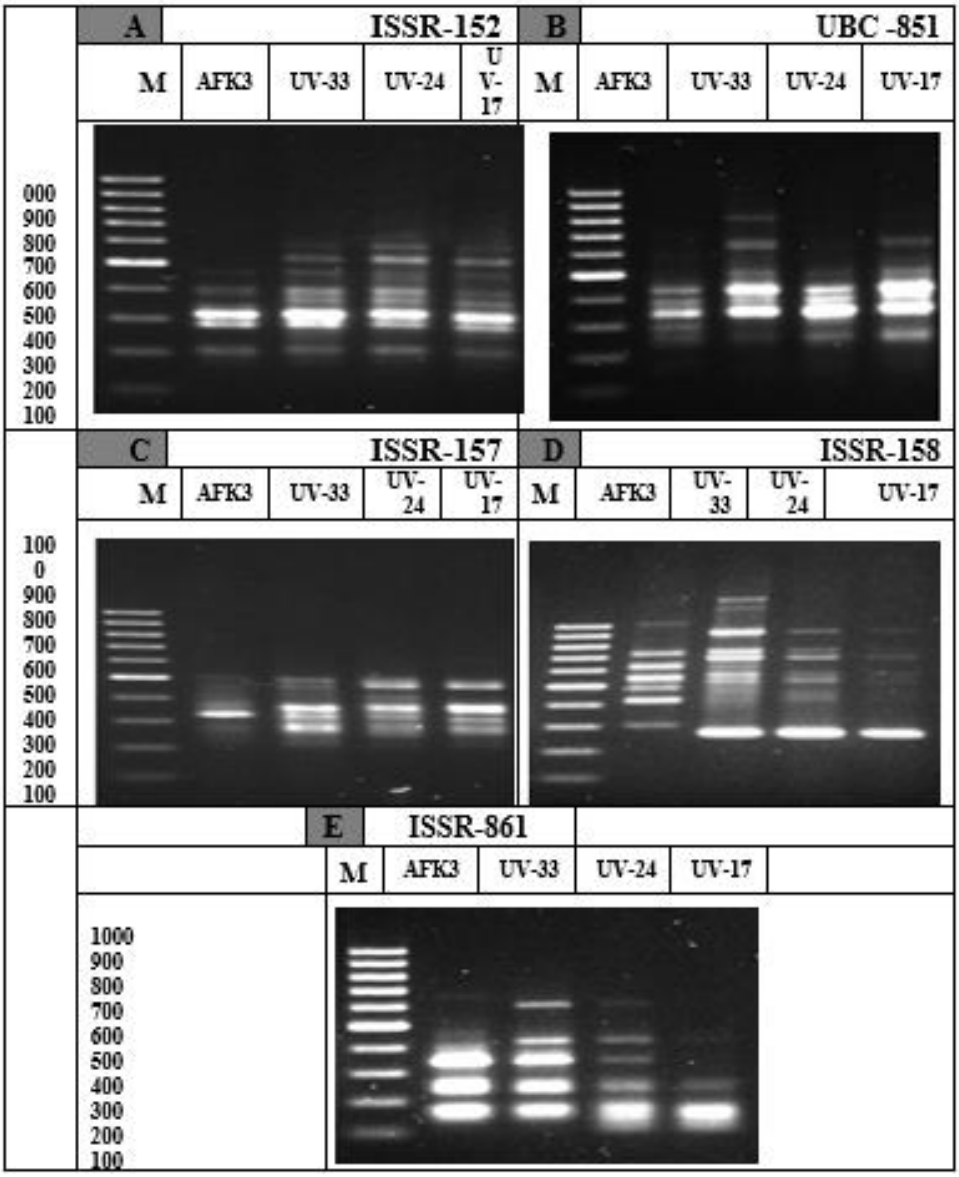

Fig.5: The Inter-Simple Sequence Repeats (ISSR) amplification pattern obtained for four samples of *Aspergillus flavus*isolate AFK3 accession number OK086056 and three mutants, a primer ISSR-152, b primer UBC-851, c primer ISSR-157, d primer ISSR-158 and e primer ISSR-861.

Table 8: Bands variation and polymorphism percentage in four samples of *Aspergillus flavus* strain AFK3 and three mutants using five ISSR primers.

Primers	Total Bands	Molecular Size (bp)	Number of Monomorphic	Number of Polymorphic+uniq.	Polymorphism %
ISSR-152	9	559-188	5	4	44%
UBC 851	9	825-271	4	5	55%
ISSR-157	9	574-195	5	4	44%
ISSR-158	15	1614-246	1	14	93%
ISSR-861	10	572-135	2	8	80%
	52		17	35	63%

Table 9: The total bands produced from each primer for all amplified fragments from *Aspergillus flavus* strain AFK3 and three mutants.

Total bands	Primers					
Genotypes	**ISSR-152**	**UBC 851**	**ISSR-157**	**ISSR-158**	**ISSR-861**	**Total**
AFk3	5	5	6	7	5	28
UV-33	8	8	6	12	6	40
UV-24	9	5	8	8	6	36
UV-17	8	7	6	6	6	33

Table 10: polymorphic with unique bands produced from each primer for all amplified fragments from four samples the strain *Aspergillus flavus* AFK3 and three mutants.

poly+unique bands	ISSR-152	UBC 851	ISSR-157	ISSR-158	ISSR-861	Total
AFk3	0	1	1	6	3	11
UV-33	3	4	1	11	4	23
UV-24	4	1	3	7	4	19
UV-17	3	3	1	5	4	16

Proximity Matrix Analysis (Genetic Similarity):

The data presented in Table 11, documented six pairwise comparisons aimed at discussing the genetic relationships among the four *Aspergillus flavus* genotypes in terms of their similarity. The genetic similarity values ranged from 0.557 to 0.842, with an average value of 0.699. The highest genetic similarity was observed between UV. -33 and UV. -24, reaching 0.842, while the lowest similarity was recorded between AFk3 and UV. -17, with a value of 0.557. Additionally, notable high genetic similarity values were noted within certain pairs, including UV-33 and UV-17 (0.822), UV-24 and UV-17 (0.841), AFk3 and UV-33 (0.647), and AFk3 and UV-24 (0.625).

Table 11: Genetic similarity percentages for strain *Aspergillus flavus* AFk3 and three mutants, using five ISSR Primers.

	***Aspergillus flavus*AFK3**	**S.A-33**	**S.A -24**	**S.A -17**
***Aspergillus flavus*AFK3**	1.000			
UV-33	0.647	1.000		
UV-24	0.625	**0.842**	1.000	
UV-17	**0.557**	0.822	0.841	1.000

Cluster Analysis (phylogenetic tree):

The outcomes of the cluster analysis, depicted in Figure 6, grouped all the *Aspergillus flavus* genotypes, which encompassed both the strain and mutants, into two primary clusters. Cluster I was composed of two sub-clusters. The sub-cluster one exclusively contained UV. -17. In contrast, sub-cluster 2 was subdivided into two further sub-clusters. The sub-cluster one consisted of a group that included UV. -24 and UV. -33. Cluster II, conversely, comprised only AFK3.

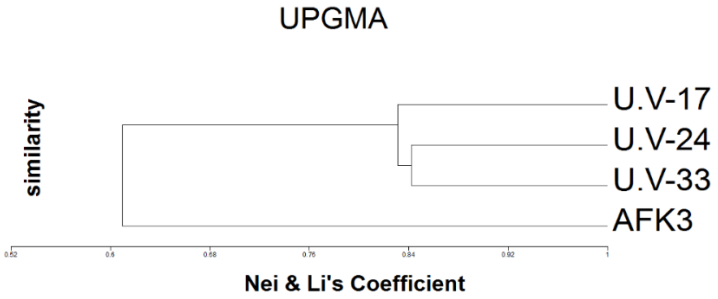

Fig 6. Dendrogram representing the genetic relationship among strain *Aspergillus flavus* AFK3 and three mutants using UPGMA cluster analysis of Nei-Li's similarity coefficient generated from the five ISSR markers.

***Subtilisin* Encoding Gene Amplification from *A. flavus AFK3* and Mutant *A. flavus* UV-33 and Alignment in Genbank (Blast):**

The primers that were designed for the subtilisin gene were successfully amplified and sequenced. Subsequently, the assembled sequence was compared to existing sequences in the NCBI database via a BLAST search. This analysis unveiled an open reading frame (ORF) of 2055 bp in length, which aligns with the expected size of the *subtilisin* gene. This ORF encodes a protein of 684 amino acids, a characteristic shared by both *A. flavus* AFK3 and mutant *A. flavus* UV-33. The results demonstrated that the *subtilisin* gene in *A. flavus* AFK3 and mutant *A. flavus* UV-33 exhibited a 99% similarity to the *subtilisin* found in *A. flavus* strain CA14. Consequently, the gene sequences responsible for encoding the *subtilisin* in *A. flavus* AFK3 and mutant *A. flavus* UV-33 were deposited in GenBank with accession numbers OQ511278 and OQ511279, respectively. Subsequently, the nucleotide sequence of the *subtilisin* gene was converted into its matching amino acid sequence, which served as the representation of the protein under investigation. The amino acid sequence was then compared to three other *subtilisin* proteins obtained from the UniProt protein database. The InterProScan server (EMBL) has identified the amino acid residues from 1 to 684 as belonging to the *subtilisin* family.

Multiple Sequence Alignments:

During the analysis of multiple sequence alignment, it was observed that the *subtilisin* gene exhibited four distinct consensus regions among the three sequences. The sequences from *A. flavus* AFK3, mutant *A. flavus* UV-33, and *A. flavus* CA14 *subtilisin* displayed a high degree of similarity, signifying their close genetic relationship within the *Aspergillus* genus. Further investigation unveiled the presence of active sites in the *subtilisin* proteins of *A. flavus* AFK3, mutant *A. flavus* UV-33, and *A. flavus* CA14, positioned at specific locations, namely ILE157, ASN319, GLN230, VAL421, and THR326. This information is visually represented in Figure 7.

G, P, S, T H, K, R F, W, Y I, L, M, V

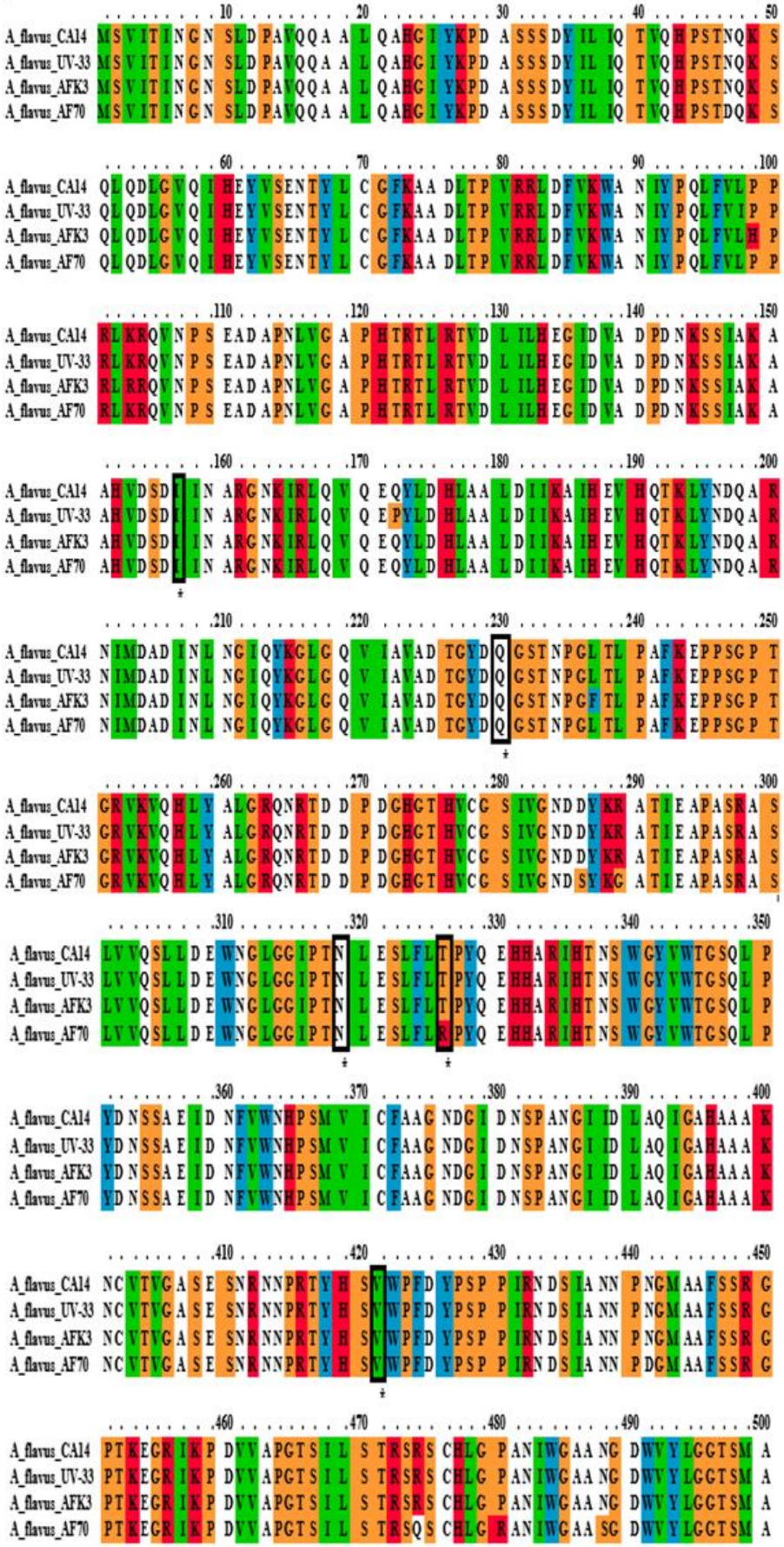

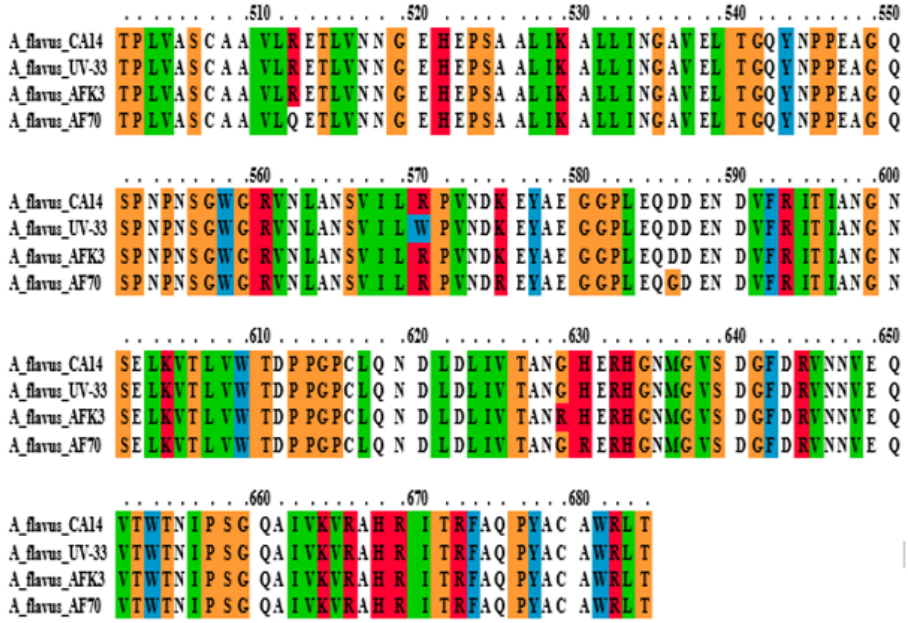

Fig. 7: Multiple sequence alignment of the experimentally determined amino acids for *subtilisin* amino acids from the *Aspergillus* family; *A. flavus AFK3*, mutant *A. flavus UV-33*, *A. flavus CA14* and *A. flavus* AF70. Amino acid sequence alignment was performed by PSI-BLAST pre-profile processing (Homology-extended alignment) available from the PRALINE online resource portal (http://www.ibi.vu.nl/programs/ pralinewww/). Active site residues across the *subtilisin* are marked with a black ‘‘*’’. The current colourscheme of the alignment is by amino acid residue type.

Cluster Analysis (phylogenetic tree) of the *A. flavus subtilisin (SUB)* Sequence:

Subsequently, a phylogenetic analysis was conducted to determine the *subtilisin* protein's placement within the known members of the *subtilisin* family. A selection of four curated *subtilisin* proteins from diverse organisms was obtained from the UniProt protein database for this phylogenetic analysis. The dataset included *subtilisin* proteins from *A. flavus*, among other organisms. The comparative analysis indicated that the *subtilisin* protein shared a high sequence similarity of 99% with homologous *subtilisin* proteins found in *A. flavus* AFK3 and mutant *A. flavus* UV-33 (e.g., *Aspergillus sp*.). For the construction of the phylogenetic tree, MEGAX software was utilized, incorporating the *subtilisin* sequences from four *Aspergillus* strains, namely *A. flavus* AFK3, mutant *A. flavus* UV-33, template *A. flavus* strain CA14 and *A. flavus* AF70. The results revealed that all *Aspergillus flavus* genotypes fell into three primary clusters. Cluster I included *A. flavus* CA14 and *A. flavus* AFK3, which exhibited a close relationship with the *subtilisin* protein. Cluster II was solely composed of mutant *A. flavus* UV-33. Cluster III contained strain *A. flavus* AF70. This arrangement is visually depicted in Figure 8.

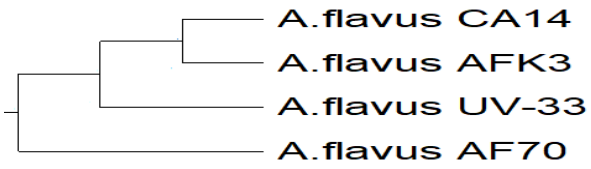

Fig. 8: Phylogenetic tree of four strians *Aspergillus subtilisin* protein sequences; template *A. flavus* strain CA14; *A, flavus AFK3*, mutant *A. flavus UV-33*, and *A. flavus* AF70, constructed using the neighbor-joining method (MEGAX) software.

Secondary Structure Prediction of *subtilisin* Protein:

The subtilisin protein from A. flavus AFK3 and mutant A. flavus UV-33 was aligned and its secondary structure predicted using the PDBsum service. Figure 9a shows the secondary structure of the subtilisin enzyme predicted for A. flavus AFK3 based on the subtilisin model characterization by PDBsum. This structure consists of 33 strands, 22 helices, 9 helix-helix interacs, 76 beta turns, and 33 gamma turns. There are also 10 sheets and 1 beta alpha beta unit. Fig. 9b shows that mutant A. flavus UV-33 has the following structural features: 9 sheets, 1 beta alpha beta unit, 5 beta hairpins, 11 beta bulges, 32 strands, 24 helices, 11 helix-helix interacs, 68 beta turns, and 24 gamma turns.

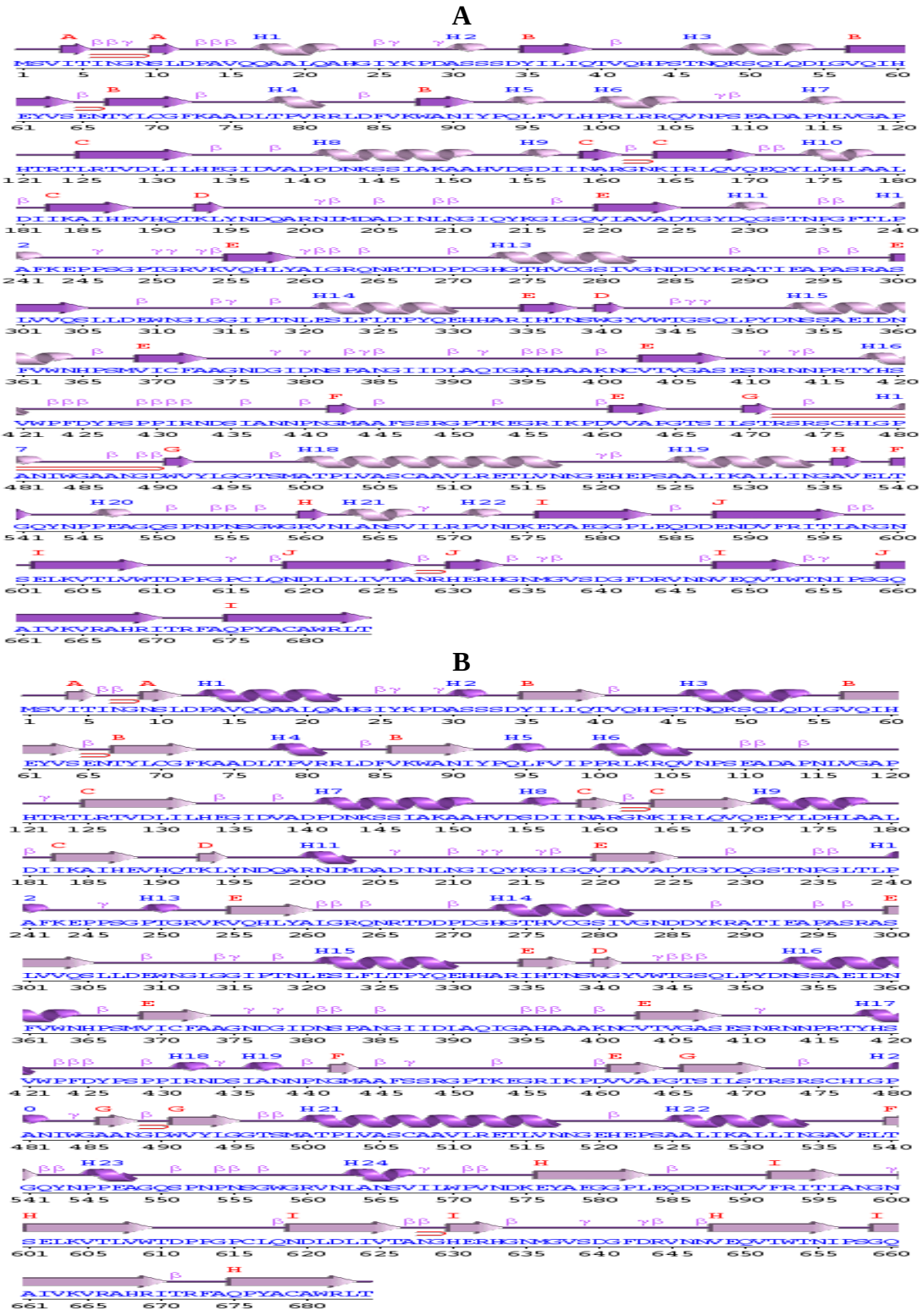

Fig. 9: predicted secondary structure of *subtilisin protein* of**: A,** *A, flavus AFK3*; **B;** mutant *A. flavus UV-33*

Homology Modelling and Validation of the *subtilisin (SUB)-Encoding* protein:

In the context of this research, I-TASSER generated five distinct models for the 684-residue three-dimensional (3D) structure of *subtilisin* proteins of *A. flavus* CA14, *A. flavus* AFK3, and mutant *A. flavus* UV-33 based on their cluster density. Nonetheless, the *subtilisin* structure from *A. flavus* AFK3 exhibited homology with the *subtilisin* protein originating from *A. flavus* CA14.

The five models generated for the template *A. flavus* CA14 yielded varying C-scores (confidence scores), Among these models, model 1, which possessed the highest C-score -3.35, was selected for further analysis. It is important to note that a higher C-score indicates a model with greater confidence, while a lower C-score implies lower confidence. The estimated TM-score for Model 1 was 0.35±0.07, and the estimated RMSD was 16.1±3.5Å, as in figures 10a. In the case of *A. flavus* AFK3, different models were generated with the C-scores. Among these models, model 1, which possessed the highest C-score -3.23, was chosen for further analysis. The estimated TM-score for Model 1 was 0.47±0.21, with an estimated RMSD of 13.4±5.2Å, as in figures 10b. Similarly, for mutant *A. flavus* UV-33, the various models generated had these C-scores. Once again, model 1, with the highest C-score -3.21, was picked for further analysis. The estimated TM-score for Model 1 was 0.49±0.22, and the estimated RMSD was 14.1±6.6Å, as presented in figures 10c.

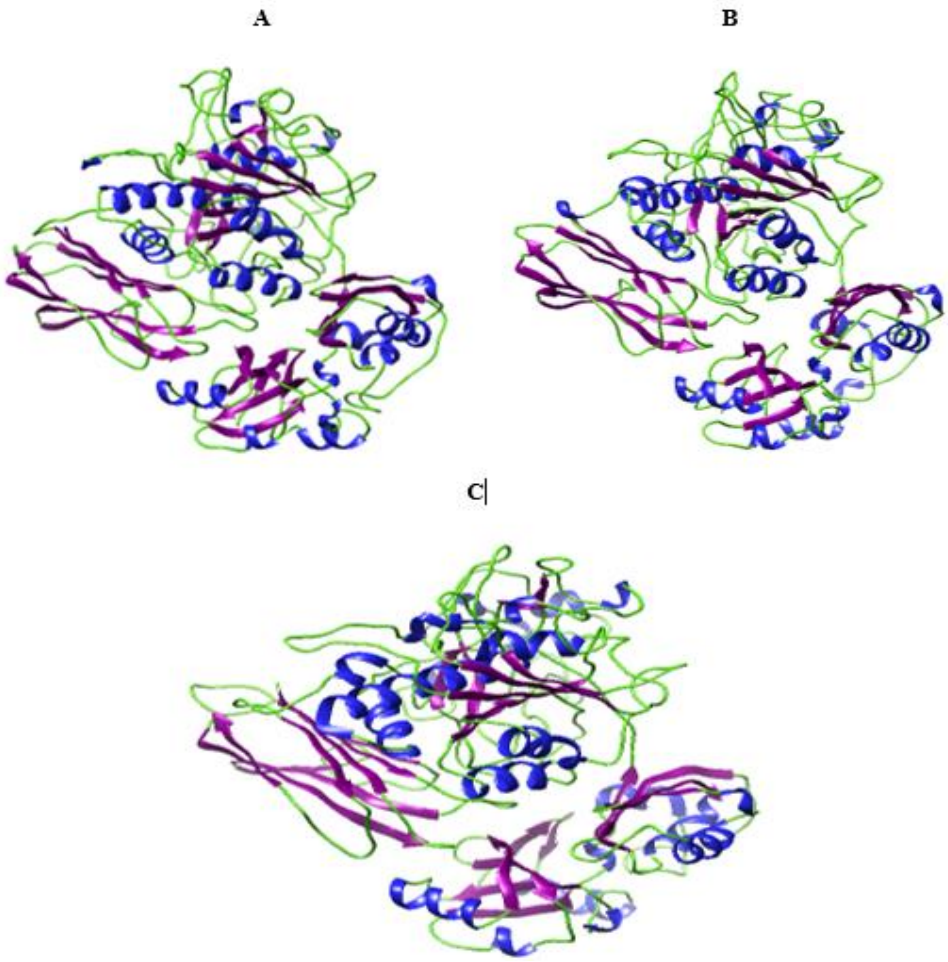

Fig.10: Modeled 3D structure of; **A,** template *A. flavus* CA14, **B,** strain *A. flavus* AFK3. **C,** mutant *A. flavus* UV-33 *subtilisin*.

The selected model underwent energy minimization using the force fields of the Swiss-PdbViewer through the YASARA Server. Subsequently, the resulting model underwent assessment using PROCHECK, VERIFY3D, and ERRAT from the SAVES server to evaluate its overall stereochemical properties. Additionally, a Ramachandran plot was generated for the energy-minimized *subtilisin* structures. The Ramachandran plot divides the x-axis into four quadrants: the low-energy region, the allowed region, the generously allowed region, and the disallowed region. For the 3D-modeled template *A. flavus* CA14 *subtilisin* protein, the PROCHECK analysis showed that 84.0% of residues were located within the most favoured regions of the Ramachandran plot. Furthermore, 12.7% of residues fell into the additional allowed regions, 1.9% in the generously allowed regions, and 1.4% in the disallowed regions, as presented in Figure 11a. Similarly, in the case of the 3D-modeled strain *A. flavus* AFK3 *subtilisin* protein, PROCHECK analysis indicated that 81.5% of residues were within the most favoured regions of the Ramachandran plot, with 15.1% in the additional allowed regions and 1.5% in the generously allowed regions. Additionally, 1.9% of residues were in the disallowed regions, as presented in Figure 11b. Regarding the 3D-modeled mutant *A. flavus* UV-33 *subtilisin* protein, the PROCHECK analysis revealed that 85.2% of residues were situated within the most favoured regions of the Ramachandran plot. Moreover, 12.2% of residues were in the additional allowed regions, 0.7% were in the generously allowed regions, and 1.9% of residues were in the disallowed regions, as presented in Figure 11c. VERIFY3D and ERRAT analyses from the SAVES server were also employed to validate the overall quality and compatibility of the atomic model (3D) with the amino acid sequence (3D-1D). The Ramachandran plot calculations confirmed that 89.58%, 92.11%, and 92.39% of the total residues of template *A. flavus* CA14, strain *A. flavus* AFK3, and mutant *A. flavus* UV-33 *subtilisin*, respectively, resided within the most favoured region. These results, combined with the findings from the ERRAT, VERIFY3D, and PROSA models, provided strong evidence of the reliability and suitability of the in-silico studies. Additional visual representations of this information can be found in Figures 11a, b, and c.

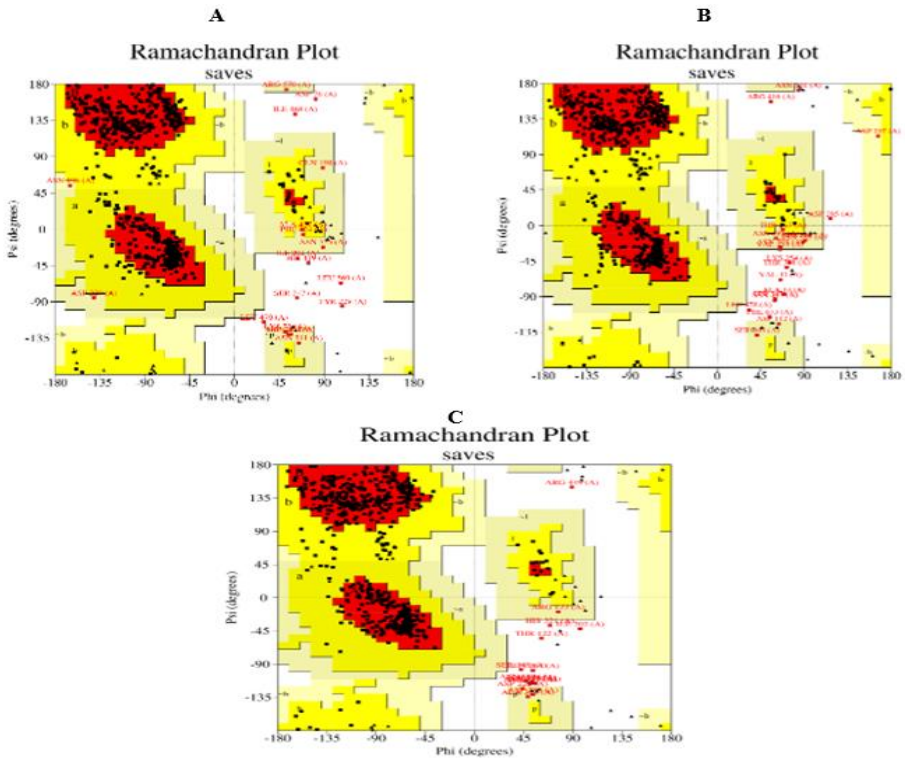

Fig 11: Ramachandran plot of; **A,** template *A. flavus* CA14, **B,** strain *A. flavus* AFK3. **C,** mutant *A. flavus* UV-33 *subtilisin.*

***Subtilisin* Binding Pocket Prediction and Sequence Analysis:**

The playmolecule/deepsite server (http://playmolecule.com/deepsite/) was employed to identify the active site amino acids. Predictions were made for the active sites of template *A. flavus* CA14 *subtilisin* and Ligand beta keratin. For Template *A. flavus* CA14 *subtilisin*, an active site with a score of 0.995 was discovered, composed of two amino acids: ILE157 and ASN319, with interface residues receiving scores of 1.753 and 1.939, respectively. In the case of Ligand beta-keratin, the active site was determined and presented, consisting of two amino acids at the Centre: LEU35 and PRO65, with interface residues receiving scores of 1.753 and 1.939, respectively. Similarly, for *A. flavus* AFK3 *subtilisin*, an active site with a score of 1.090 was identified, comprising two amino acids: GLN230 and VAL421, with interface residues scores of 1.789 and 1.023, respectively. The active site for Ligand beta keratin was also predicted, including three amino acids at the active site centre: GLN37, TYR73, and TYR77, with interface residues had scores of 1.789, 1.023, and 1.849, respectively. Regarding mutant *A. flavus* UV-33 *subtilisin*, an active site with a score of 0.990 was located, featuring one amino acid at the active site centre: THR326, with interface residue receiving a score of 1.768. The active site for Ligand beta-keratin was identified as well, consisting of one amino acid at the active site center: GLY81, with interface residue, and received a score of 1.768. These findings offer valuable insights into the active sites of the *subtilisin* proteins and their interactions with the Ligand beta-keratin.

Comparison of *SUB* protein sequence analysis of the *A. flavus* AFK3 and mutant *A. flavus* UV-33 strains, showed four substitutions of GLN172PRO, PHE237LEU**,** ARG570TRP and ARG629GLY in *A. flavus* AFK3, mutant *A. flavus* UV-33, that led to an improvement of the catalytic efficiency of keratinase by mutant strain compared with the wild type, as described in Figure 12.

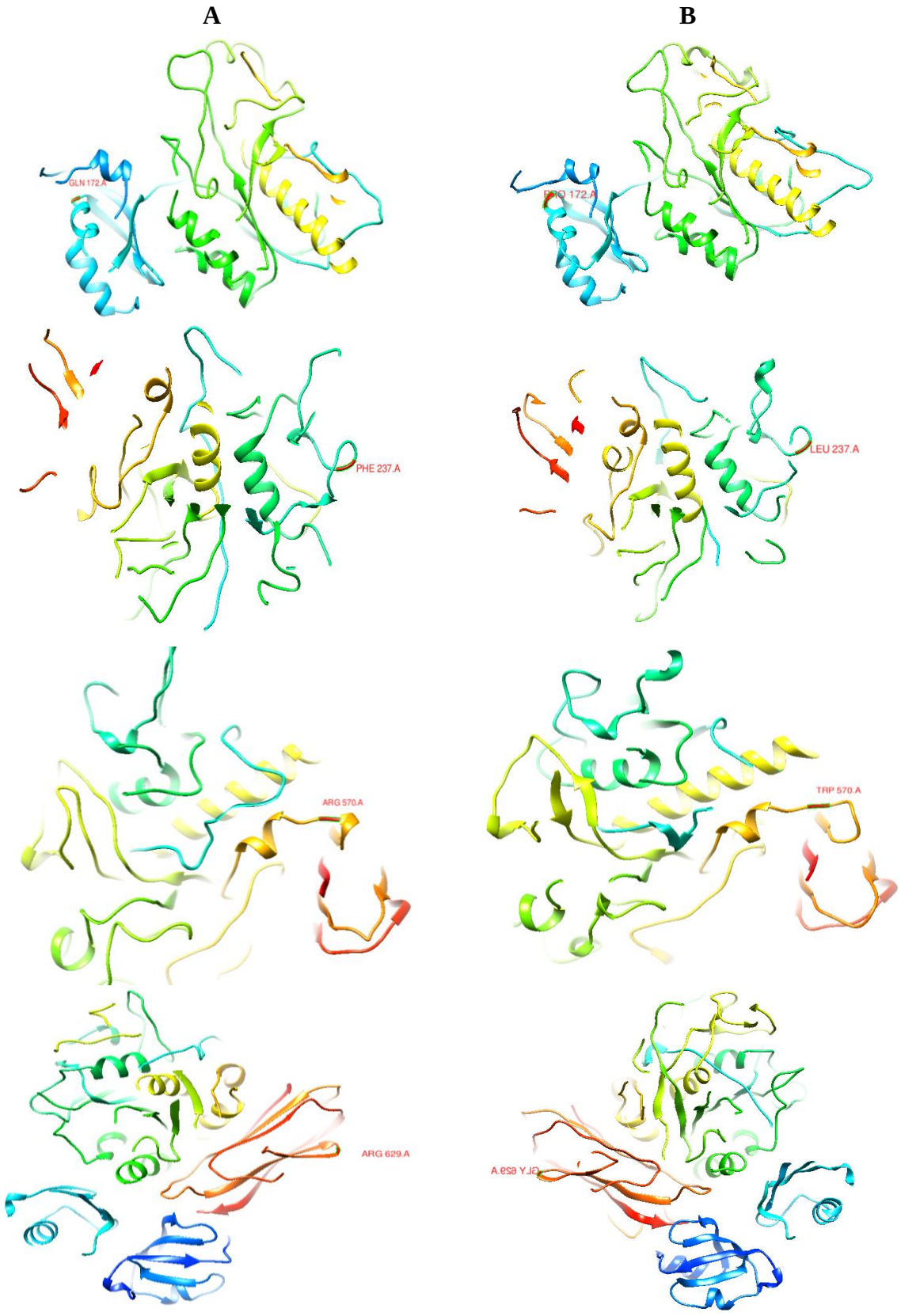

Fig. 12: Amino acid substitution of *subtilisin* of; wild GLN172PRO mutant, wild PHE237LEU mutant, wild ARG570TRP mutant and wild ARG629GLY mutant, in red color, of; **A;** wild type *A. flavus* AFK3 and **B;** mutant ***A. flavus*** UV-33.

Docking and Molecular Interaction Studies:

Using the HDock web-based programme, docking experiments were conducted to investigate the substrate-protein binding mechanism of subtilisin with keratin. For the docking technique, the macromolecule's receptor and ligand files were saved in PDB format. The Gasteiger type was used to assign polar hydrogen charges, and carbons were combined with nonpolar hydrogen atoms. The torsions and internal degrees of freedom were modified appropriately. A three-dimensional model of subtilisin was used to summarise the docking findings of beta-keratin with the model. Template A. flavus CA14 subtilisin showed an interaction with -277.11 kcal/mol affinity, 0.9270 confidence, 53.60 ligand rmsd (Å), and 1.753 interface residue scores for receptor ILE157 and ligand LEU35. Furthermore, as seen in Figure 13a, the receptor ASN319 and ligand PRO65 active site amino acids displayed interface residues with a score of 1.939. Interface residues associated with this interaction score of 1.789 were found in the active site amino acids of receptor GLN230 and ligand GLN37, and the results for A. flavus AFK3 subtilisin indicated an interaction with an affinity score of -274.06 kcal/mol, a confidence score of 0.9228, and a ligand rmsd () of 63.83. In addition, as shown in Fig. 13b, the active site amino acids of receptor VAL421 and ligand TYR73 had interface residues with a score of 1.023, and the active site amino acids of receptor VAL421 and ligand TYR77 had interface residues with a value of 1.849. An interaction was found between the mutant A. flavus UV-33 subtilisin and the receptor THR326 and ligand GLY81, according to the data. The interaction had a confidence score of 0.9553, an affinity score of -303.13 kcal/mol, and a ligand rmsd () of 71.73. According to Figure 13c, the interface residue or residues involved in this interaction obtained a score of 1.768.

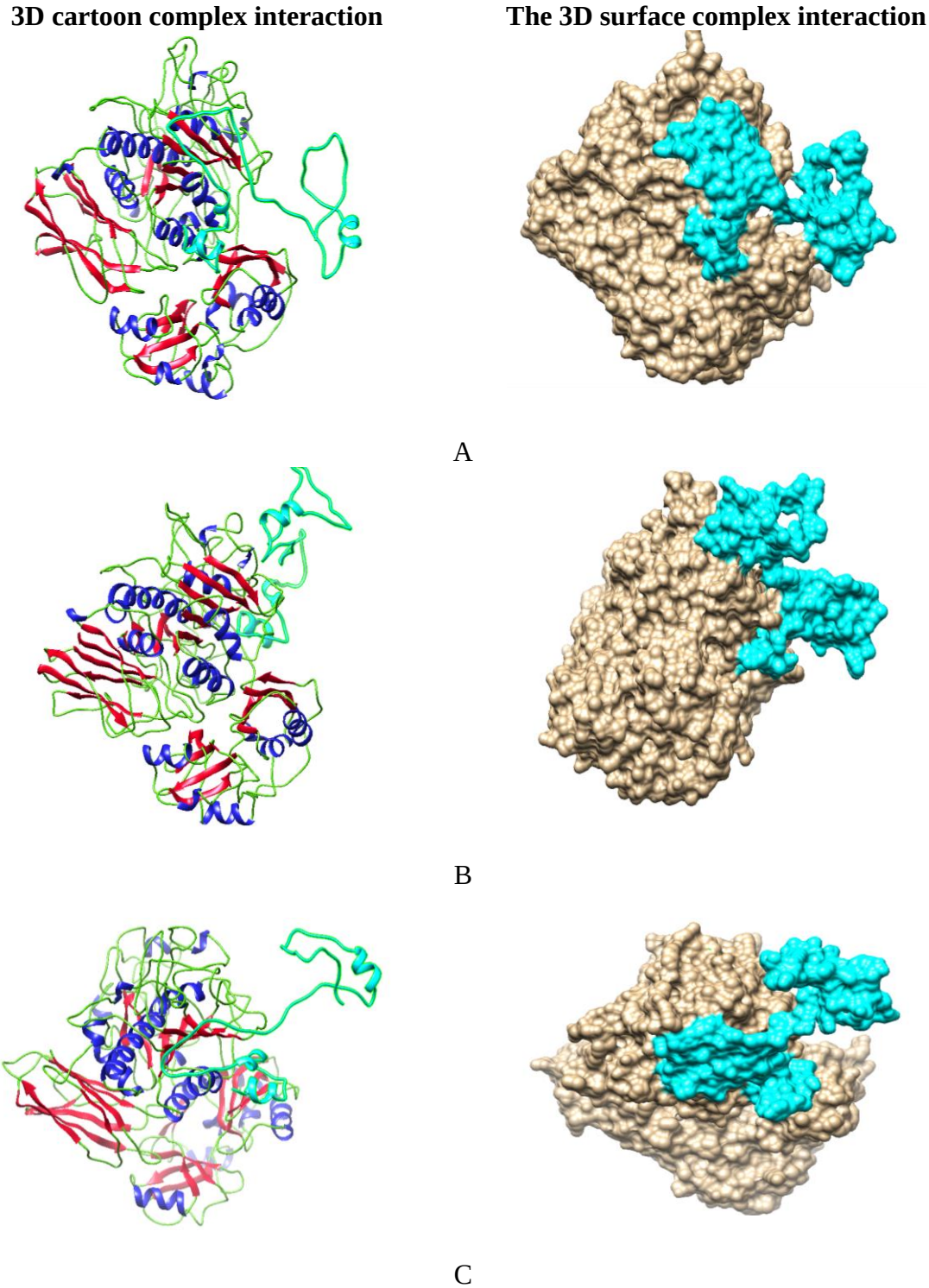

Fig. 13: Molecular 3D cartoon and surface model complex interaction of ligand beta keratin (cyan colour) with *subtilisin* amino acids of **A;** ***A. flavus*** CA14. **B;** *A. flavus* AFK3 **C;** mutant *A. flavus* UV-33, in active sites with the best binding mode in the pocket of the protein.

DISCUSSION

Various methods are employed to induce random mutations in microorganisms, such as mutagenesis using mutagenic agents and transposons. Random mutagenesis is a common practice for developing mutants, but it is a labour-intensive trial-and-error process. The main effect of mutagenic agents including X-rays, UV-rays, nitrous acid, dimethyl

sulphonate, ethyl methane sulfonate, hydrogen peroxide, sodium azide and acridine mustards, is to create lesions or modifications in the DNA sequence (structure genes or colony characteristics or loss in sensitivity to antibiotics or regulatory genes), leading to changes in gene function or generally a change in the end-product specified by that gene, which potentially resulting in beneficial traits. However, the mutagenic process is not targeted, requiring screening of numerous mutants to identify desired phenotypes **(**Akbar *et al*., 2013; Xin 2012; Almahasheer *et al*., 2022 Lateef *et al*., 2018).

In this study, various fungal strains were assessed for keratinase production, with *A. flavus* AFK3 exhibiting the highest activity at 62.15 U/ml. To enhance keratinase expression in this strain, physical UV, and chemical mutagenesis (EMS and SA) were employed. This resulted in the generation of a stable mutant, UV-33, which showed increased keratinolytic activity (115.7 U/ml) compared to the wild type. This mutant could be useful for biotechnological applications in keratinase production and feather waste utilization.

Previously, *A. niger's* α- and β-galactosidases were genetically enhanced using gamma-ray-induced mutagenesis, resulting in a two-fold increase in enzyme activity (Siddique *et al*., 2011). *Ashbya gossypii* was improved using random mutagenesis with EMS, yielding mutants like S436 with 1.4- to 2-fold increases in all measured enzymatic activities compared to the parent strain, while other mutants showed 2- to 3-fold improvements in specific activities (Ribeiro *et al*., 2013). *Streptomyces werraensis* KN23 underwent sequential mutagenesis with UV, SA, and H_2O_2, resulting in several mutants, with SA-27 exhibiting high keratinase activity at 106.92 U/ml (Khalil *et al*., 2022).

Response surface methodology (RSM) to concurrently examine the main and interaction impacts of several environmental conditions on the production of keratinase. Response surface methodology (RSM) was used to optimize keratinase production in *A. flavus* AFK3, reaching 133.73 U/ml by maintaining a pH of 7, an incubation time of 72 hours, and adding 1.5% fructose and 1.5% malt extract. Similarly, mutant *Pichia kudriavzevii* EMS-37 achieved 240.172 U/ml keratinase activity (Khalil *et al*., 2022). *Curvularia lunata* attained 123 U/ml keratinase activity in solid-state fermentation (Kumar and Yadav 2022), and *Aphanoascus fulvescens* B21/4-5 reached a maximum substrate mass loss of 71.08% under optimized conditions (Bohacz 2017). *A. stelliformis*, *A. sydowii*, and *Fusarium brachygibbosum* exhibited keratinase activities of 113, 120, and 130 IU mg -1, respectively (Suaad *et al*., 2021). *Penicillium chrysogenum* produced laccase with an optimum activity of 6.0 U/ml (Senthivelan *et al*., 2019).

Inter Simple Sequence Repeat (ISSR) markers, a PCR-based method, are highly polymorphic and useful in genetic diversity, phylogeny, gene tagging, genome mapping, and evolutionary biology studies (Salim *et al*., 2019). These markers, like ISSR-PCR, offer a quick, cost-effective, and reproducible way to characterize genetic variation. While ISSR markers are not directly related to enzyme activity, they can indirectly impact it by reflecting genetic diversity and population structure within a species. This technique is widely used in plants, yeasts, and bacteria for its effectiveness in identifying genetic differences among strains (Salim *et al*., 2019).

In this study, *A. flavus* AFK3 shows promise for keratinase production despite its eukaryotic origin. ISSR-PCR markers were used to differentiate between strains, revealing 52 markers with 35 polymorphic bands (63%). In terms of polymorphic bands, UV-33 had 23 unique bands. Compared to wild type AFK3 had fewer total bands (28) and polymorphic bands (11). ISSR analysis identified nucleotide sequence variations between mutants and

wild-type AFK3. Other studies have also used ISSR to identify and differentiate *Aspergillus* species (Salim *et al*., 2019), assess genetic diversity (Abbas *et al*., 2020), and categorize strains based on geographical origin and species (Arra *et al*., 2015). A study on *A. alternata* identified six distinct groups using ISSR markers (Mohammadi and Bahramikia 2019).

To compare the differences in keratinase enzyme activity between the wild type and its mutant resulting from mutation induction, the keratinase *subtilisin* gene must be isolated and sequenced from both strain and mutant. This comparison should involve nucleotide and protein-level comparisons, including multiple sequence alignment, protein secondary and three-dimensional structure analysis, protein validation, amino acid substitution, and molecular docking studies.

Keratinases are classified based on their active site as *serine proteases*, *alkaline proteases*, and *metalloproteases* (Gurunathan *et al*., 2021). Some keratinases, including those from *A. flavus* K-03, belong to the *serine proteases* (S8 family) and the superfamily of *subtilisin*-like proteases with an active *serine* centre. The keratinase of *A. flavus* AFK3 and mutant *A. flavus* UV-33 is determined to be the *subtilisin* gene (*SUB*), exhibiting 99% similarity with the *subtilisin* of the *A. flavus* strain CA14.

In related studies, the keratinase gene from *Bacillus licheniformis* MZK-05, *Bacillus licheniformis* BBE11-1, and *Bacillus licheniformis* KRLr1 were successfully amplified and sequenced. Additionally, the keratinase genes from the *B. cereus* group, thermitase *alkaline serine protease*, and thermophilic *serine protease* showed high similarity with the keratinase KerS gene. The kerT1 gene (1170 bp) from *Thermoactinomyces sp*. YT06, feather-degrading bacteria, was also effectively amplified (Kim 2007; Nahar *et al*., 2016; Peng *et al*., 2010; Rahimnahal *et al*., 2023; Wang *et al*., 2019).

In this investigation, variations in the active site location were observed among different strains of *A. flavus subtilisin*. Multiple sequence alignment of *A. flavus* AFK3, mutant *A. flavus* UV-33, and *A. flavus* CA14 *subtilisin* sequences revealed high similarity between AFK3, UV-33, and CA14. (Peng *et al*., 2021) Reported pro-peptide sequence alignment of keratinases, obtaining eight highly expressed and active keratinase sequences for recombinant keratinase KerZ1. (Rahimnahal *et al*., 2023) Reported protein sequence alignment of keratinase *B. licheniformis* KRLr1 with closely related sequences. Multiple amino acid sequence analysis of the KerS gene against S8 family peptidase *Bacillus cereus* group sequences obtained from GenBank showed 19 amino acid substitutions, enhancing the protease by approximately 31.17%, with nine substitutions increasing catalytic efficiency (Almahasheer *et al*., 2022; Abdel-Naby *et al*., 2022).

In our investigation, a phylogenetic tree was constructed using MEGAX software to analyze the relationships between strains of *A. flavus* subtilisin protein. *A. flavus* AFK3 and mutant *A. flavus* UV-33 showed the highest similarity to *A. flavus* CA14. Phylogenetic analysis of KRLr1 and related sequences showed the highest similarity to *B. licheniformis* keratinase, a member of the serine peptidase/subtilisin-like S8 family (Rahimnahal *et al*., 2023**)**. The unrooted neighbor-joining (NJ) tree was constructed based on high similarity in protein sequence alignment.

A polypeptide's local spatial conformation apart from its side chains is known as its secondary structure. A variety of regular secondary structures, with lengths ranging from α-helices to β-sheets and twists, are often seen. An example would be the fact that α-helices and β-sheets may have anywhere from three to more than fifty residues. The topology of a protein's structure explains how its secondary components are linked to one

another. As an example, the βαβ topology describes a section of a protein that consists of a β-strand linked to an α-helix and then another β-strand. Topology diagrams are useful for β-sheet categorization because they depict the two-dimensional secondary structure of a polypeptide chain, including all its parts, and how they are connected to each other and to their neighbours.

According to the PDBsum characterization, there are differences in the predicted *subtilisin* enzyme's topology and secondary structure between *A. flavus* AFK3 and mutant *A. flavus* UV-33. (Rahimnahal *et al*., 2023) Reported that KRLr1 has a secondary structure with 25% α-helix and 27% β-sheet content according to NetSurfP-2.0. The predicted active site cleft of KRLr1 includes amino acids in proximity to the *B. subtilis subtilisin* E structure, such as His75, Asp136, Asn138, His140, Leu172, Ser175, Ser177, Ser232, Ala279, Thr292, Ans294, and Ser297.

A protein's tertiary structure is the three-dimensional arrangement of all atoms, including the functional groups' locations and the spatial coordination of components in the secondary structure. To better understand how proteins interact with ligands and other molecules, it is essential to have access to 3D structure prediction tools that can model protein sequences with unknown structures. Tools like I-TASSER are dependable for modelling protein sequences without known structural data, aiding in understanding the relationship between protein sequences, structures, dynamics, and functions (Xu and Yang 2013).

In this study, I-TASSER, ROBETTA, and Phyre2 were used for homology modelling of *subtilisin* proteins from *A. flavus* CA14, *A. flavus* AFK3, and mutant *A. flavus* UV-33 (Kathwate 2020; Heo *et al*., 2013). I-TASSER, an interactive framework that predicts protein structure and function using templates, refines the structure depending on the target protein sequence and then builds full-length atomic structural models using the most significant template. (Kulkarni and Devarumath 2014; Zhang 2008). LOMETS is used within I-TASSER to generate five models, with the best model selected based on a confidence score (C-score) and potential energy for further analysis (Singh and Muthusamy 2013; Roy *et al*., 2012; Zheng *et al*., 2021). The C-score, ranging from -5 to 2, indicates the model's quality, with higher scores indicating greater confidence and reliability (Yang and Yang 2015; Patni *et al*., 2021). Five models were generated using I-TASSER for the 684-residue *subtilisin* protein of the template *A. flavus* CA14, *A. flavus* AFK3 and mutant *A. flavus* UV-33. Model 1 of both strains was selected based on the highest C-score, indicating a high confidence level. These models were based on their cluster density (Zheng *et al*., 2021), and were selected for further analysis (Yang and Yang 2015).

The subtilisin structure was validated using SAVES v6.0, which includes VERIFY-3D for 3-D sequence profile assessment and PROCHECK for structure validation via Ramachandran plots (Patni *et al*., 2021; Beg *et al*., 2018). The Ramachandran plot divides the x-axis into four regions: low energy, allowed, generously allowed, and disallowed. Validation Ramachandran plot scores indicate accurate protein modelling with certain amino acids in the favoured region or inaccurate modelling with certain amino acids outside the favoured region.

The *subtilisin* proteins of *A. flavus* AFK3 and mutant *A. flavus* UV-33 displayed a high percentage of residues in the most favoured region of the Ramachandran plot, indicating stability. Predicted active sites for these strains contained distinct amino acids at their cores (Kesharwani and Misra 2011). Homology modelling with the Swiss-Model program estimated the structure of keratinase KerZ1, revealing specific structural elements. α-helices and β-sheets, crucial for protein structure and function, were identified (Waterhouse *et al*., 2018; Marcos *et al*., 2018). I-TASSER predicted a viable

topological model for KerZ1, with validation showing high accuracy. Modeller V.9 refined the structure of the *Bacillus subtilis* keratinase KRLr1, with quality factors indicating accurate modelling. A Ramachandran plot demonstrated a high percentage of the allowed region for the keratinase 3D structure, confirming the accuracy of the model (Almahasheer et al., 2022; Patni *et al*., 2021).

Differences in *subtilisin* proteins between wild-type *Aspergillus flavus* AFK3 and mutant *A. flavus* AFK3 UV-33 were examined, revealing four amino acid substitutions (GLN172PRO, PHE237LEU, ARG570TRP, ARG629GLY) in the mutant. These substitutions, resulting from mutagenic agents, altered the protein's secondary and tertiary structure, affecting its function, and leading to high efficiency in keratinase activity for keratin hydrolysis. Molecular docking studies showed higher affinity scores for the mutant (−303.13 kcal/mol) compared to the wild type (−274.06 kcal/mol) when keratinase *subtilisin* docking with ligand beta keratin, indicating increased interaction and high efficiency in keratinase activity which led to high-efficiency keratin hydrolysis (Banerjee *et al*., 2014; Gupta *et al*., 2017; Karumuri *et al*., 2015).

In a study by (Fang *et al*., 2016), *Stenotrophomonas sp.* keratinase docking was reported to increase catalytic efficiency. Protein-protein docking by (Patni *et al*., 2021) using pyDock modelled the interaction between PE_PGRS39 and the SH3 domain and integrins. (Almahasheer *et al*., 2022) Compared the predicted structure of the mutant D137N of KerS13uv+ems and seven mutants of KerS26uv to the wild type, showing an increase in binding for the mutants.

Conclusion

In conclusion, our study emphasizes the importance of keratinases in efficiently degrading keratin-rich waste like feathers. We isolated a highly productive fungal isolate, *A. flavus* AFK3, which recorded 62.15 U/ml and deposited in the NCBI database. Through mutagenesis, including UV radiation, EMS, and SA, we developed the UV-33 mutant strain with exceptional keratinase activity at 115.7 U/ml. Culture condition optimization using RSM further increased the UV-33 mutant's keratinase productivity to 133.73 U/ml under specific conditions. Genetic diversity analysis using ISSR-PCR compared *A. flavus* strain AFK3 with three mutants. The *subtilisin* 3D structure model was validated using Ramachandran's plot, showing high favorability for the template protein *A. flavus* CA14, *A. flavus* AFK3, and mutant *A. flavus* UV-33 of 89.58%, 92.11%, and 92.39%, respectively. Molecular docking studies revealed strong interactions for the template *A. flavus* strain CA14, wild type *A. flavus* AFK3, and mutant *A. flavus* UV-33 *subtilisin* with of -277.11, -274.06 and -303.13 kcal/mol, respectively. Overall, this research provides valuable insights into improving keratin-rich waste utilization and the diverse applications of keratinases in biotechnology, promoting more sustainable waste management practices.

List of abbreviations

SUB	*Subtilisin*
A. flavus	*Aspergillus flavus*
ME	Malt Extract Medium
FMBM	Feather Meal Basal Medium
UV	Ultraviolet
EMS	Ethyl Methanesulfonate
SA	Sodium Azide
RSM	Response Surface Methodology
ISSR	Inter-Simple Sequence Repeat
PCR	Polymerase Chain Reaction
NCBI	National Center for Biotechnology Information
C-Score	Confidence Score
MOE	Molecular Operating Environment
BLAST	Basic Local Alignment Search Tool
ORF	Open Reading Frame

MSA	Multiple Sequence Alignment
EMBL	European Molecular Biology Laboratory
MEGAX	Molecular Evolutionary Genetics Analysis
I-TASSER	Iterative Threading Assembly Refinement
TM-score	Template Modeling score
RMSD	Root Mean Square Deviation

Declarations

Ethics Approval and Consent to Participate: Ten different poultry waste samples were collected from ten different local poultry markets with permission to collect samples from Cairo City, Egypt.

Consent for publication: Not applicable.

Availability of data and materials: The National Centre for Biotechnology Information (NCBI) database holds the sequenced identity of Aspergillus flavus AFK3 under accession number OK086056, and the sequenced subtilisin genes under accession numbers OQ511278 and OQ511279. Within the article, you will discover all the remaining evidence that supports the conclusions of this research.

Conflict of interest: The authors declare no competing interests.

Funding: This work was supported by the Microbial Genetic Department, Microbial Chemistry Department, Biotechnology Research Institute, National Research Centre, Dokki, Cairo, Egypt.

Author Contributions: N. M. A., **B. E. K., and N. N. E.** contributed experimental procedures for the isolation of keratinase-producing fungi, assay of keratinase activity, mutagenesis experiments, and optimization of culture condition, participant data illustration, statistical analysis, article writing, revising, and editing these sections. **H. F. I.** contributed experimental procedures for molecular markers, participant data illustration, statistical analysis, article writing, revising, and editing this section. **N. M. A.** contributed experimental procedures for *subtilisin* gene amplification, 3D homology modelling, validation, molecular docking studies, participant data illustration, statistical analysis, article writing, revising, and editing these sections.

Acknowledgements: We thank the National Research Centre, Cairo Egypt for its continuous help.

REFERENCES

Abbas, A., Hussien, T. & Yli-Mattila. T. (2020). A polyphasic approach to compare the genomic profiles of aflatoxigenic and non-aflatoxigenic isolates of *Aspergillus* section Flavi. *Toxins,* 12(1), 56

Abdel-Naby, M.A., El-Wafa, W.M. & Salim, G.E. (2020). Molecular characterization, catalytic, kinetic, and thermodynamic properties of protease produced by a mutant of *Bacillus cereus*- S6-3., *International Journal of Biological Macromolecules*, 160, 695–702

Abirami, S., Ragavi, R. & Antony, V.S. (2020). Utilization of keratinolytic *Lichtheimia corymbifera* AS1 for degradation of cattle hoove—A slaughterhouse waste to use in plant growth. *Biointerface Research in Applied Chemistry,* 10, 6417-6426.

Akbar, S., Prasuna, G.R. & Rasheed, K. (2013). Multistep mutagenic strain improvement in *Aspergillus carbonarius* to enhance pectinase production potential. *International Journal of Applied Biology and Pharmaceutical Technology*, 4 (2): 92-98.

Akbar, S., Prasuna, R.G. & Khanam. R. (2015). Strain improvement by induction of mutagenesis for hyper production of pectinase using *Aspergillus tamari*. *Journal of Scientific and Industrial Research,* 74:151-160.

Akram, F., ulHaq, I. & Jabbar, Z. (2020). Production and characterization of a novel thermo-and detergent

stable keratinase from *Bacillus sp*. NKSP-7 with perceptible applications in leather processing and laundry industries. *International Journal of Biological Macromolecules*, 164, 371–383.

Almahasheer, A.A., Mahmoud, A., El-Komy, H., Alqosaibi, A.I., Aktar, S., AbdulAzeez, S. & Borgio, J.F. (2022). Novel feather degrading keratinases from *Bacillus cereus* group: biochemical, genetic and bioinformatics analysis. *Microorganisms*, 10(1):93.

Arra, Y., Saini, K., Maganti, S., Babu, P.K., Laha, G.S., Madhav, M.S. & Reddy, S.M. (2015). Determination of genetic variation by using ISSR markers in toxigenic strains of *Aspergillus* in paddy from Telangana State, India. *International Journal of Agricultural Science Research*, 5(2):193-202

Bagewadi, Z.K., Mulla, S.I. & Ninnekar H.Z. (2018). Response surface methodology-based optimization of keratinase production from *Trichodermaharzianum* isolate HZN12 using chicken feather waste and its application in dehairing of hide. *Journal of Environmental Chemical Engineering*, 6, 4828–4839.

Banerjee, A., Sahoo, D.K., Thatoi, H., Pati, B. R., Mondal, K. C., Sen, A. & Mohapatra, P. K. (2014). Structural characterization and active site prediction of bacterial keratinase through molecular docking. *Journal of Bioinformatics*, 4:67–82.

Barman, N.C., Zohora, F.T., Das, K.C., Mowla, M.G., Banu, N.A., Salimullah, M. & Abu Hashem, (2017). A. Production, partial optimization and characterization of keratinase enzyme by *Arthrobacter* sp. NFH5 isolated from soil samples. *AMB Express*,7(181): 1-8.

Beg M.A., Shivangi T.S.C. & Meena L.S. (2018). Structural prediction, and mutational analysis of Rv3906c gene of Mycobacterium tuberculosis H37Rv to determine its essentiality in survival. Advances in Bioinformatics. 2018: 6152014.

Bhari, R. & Kaur, M. (2023). Fungal Keratinases: Enzymes with Immense Biotechnological Potential. In: Singh, I., Rajpal, V.R., Navi, S.S. (eds) Fungal Resources for Sustainable Economy. Springer, Singapore.

Bohacz, J., Korniłłowicz-Kowalska, T., Kitowski, I. & Ciesielska, (2020). A. Degradation of chicken feathers by *Aphanoascus keratinophilus* and *Chrysosporium tropicum* strains from pellets of predatory birds and its practical aspect. *International Biodeterioration and Biodegradation*, 151, 104968.

Bohacz. J. (2017). Biodegradation of feather waste keratin by a keratinolytic soil fungus of the genus *Chrysosporium* and statistical optimization of feather mass loss. *World Journal of Microbiology and Biotechnology*, 33(13);1-16

Bradford, M.M. (1976). A rapid and sensitive method for the quantitation of microgram quantities of protein utilizing the principle of protein-dye binding. *Analytical Biochemistry*, 72:248-254.

Cai, C., Lou, B., & Zheng, X. (2008). Keratinase production and keratin degradation by mutant strain of *Bacillus subtilis*. *Journal of Zhejiang University SCIENCE* B, 9(1):60–67.

Duarte, T.R., Oliveira, S.S., Macrae, A., Cedrola, S.L., Mazotto, A.M., Souza, E.P. Melo, A.C.N. &

Vermelho, A.B. (2011). Increased expression of keratinase and other peptidases by *Candida parapsilosis* mutants, *Brazilian Journal of Medical and Biological Research,* 44: 212-216.

El-Ghonemy, D.H., & Ali, T.H. (2017). Optimization of Physico-Chemical Parameters for Hyper Keratinase Production from a Newly Isolated *Aspergillus sp*. DHE7 using Chicken Feather as Substrate-Management of Biowaste, *Journal of Applied Pharmaceutical Science*, 7 (9):171-178.

Eramian, W., Shen, M., Pieper, U., & Sali, (2006). A. Comparative protein structure modeling using MODELLER. *Current Protocols in Bioinformatics*, 5: 1-5: 6.

Fang, Z., Zhang, J., Liu, B., Du, G. & Chen, J. (2016). Enhancement of the catalytic efficiency and thermostability of *Stenotrophomonas sp*. keratinase KerSMD by domain exchange with KerSMF. *Microbial Biotechnology*, 9:35–46.

Gafar, A., Khayat, M.E., Ahmad, S.A., Yasid, N.A., & Shukor, M.Y. (2020). Response surface methodology for the optimization of keratinase production in culture medium containing feathers by *Bacillus sp*. UPM-AAG1. *Catalysts*, 10, 848.

Gradisar, H., Friedrich, J., Križaj, I., & Jerala, R. (2005). Similarities and specificities of fungal keratinolytic proteases: comparison of keratinase of *Paecilomyce smarquandii* and *Doratomyces microsporus*to some known proteases. *Applied and Environmental Microbiology*, 71(7):3420–3426.

Gunyar, O.A., Kiraç, S., Aldi, B., & Ergin, C. (2020). Isolation, and identification of keratinophilic fungi in soil samples from excavation area of ancient city of Stratonikeia, Turkey and determination of its enzyme potentials. *Journal of Environmental Biology*, 41, 1521–1525.

Gupta, S. & Singh, R. (2013). Statistical modeling, and optimization of keratinase production from newly isolated *Bacillus subtilis* RSE163. *International Journal of Advanced Biotechnology Research*, 4(1): 167-174.

Gupta, S., Paru, T., Misri, J. & Singh, R. (2017). Molecular modeling of cloned *Bacillus subtilis* keratinase and its insinuation in psoriasis treatment using docking studies. *Indian Journal of Microbiology.* 57(4):485–491.

Gurunathan, R., Huang, B., Ponnusamy, V.K. *et al.* (2021). Novel recombinant keratin degrading subtilisin like serine alkaline protease from *Bacillus cereus* isolated from marine hydrothermal vent crabs. *Scientific Reports,* 11, 12007.

Hassan, M.A., Abol-Fotouh, D., Omer, A.M., Tamer, T.M., & Abbas, E. (2020). Comprehensive insights into microbial keratinases and their implication in various biotechnological and industrial sectors: A review. *International Journal of Biological Macromolecules* 154, 567–583.

Heo, L., Park H, Seok C. (2013). Galaxy Refne: protein structure refinement driven by side-chain repacking. *Nucleic Acids Research*, 41:384– 388.

Kamalambigeswari, R., Alagar, S. & Sivvaswamy, N. (2018). Strain improvement through mutation to enhance pectinase yield from *Aspergillus niger*and molecular characterization of *polygalactouronase* gene.

Pharmaceutical Sciences and Research, 10(5): 989-994.

Karumuri, S., Singh, P. K. & Shukla, P. (2015).In silico analog design for terbinafine against *Trichophyton rubrum*: a preliminary study. *Indian Journal of Microbiology*, 55:333–340.

Kathwate, G.H. (2020). In silico design and characterization of multiepitopes vaccine for SARS-CoV2 from its Spike proteins, *bioRxiv*, 56:1115–1135.

Kesharwani, R.K. & Misra, K. (2011). Prediction of binding site for curcuminoids at human topoisomerase II a protein; an in-silico approach. *Current Scienc,e* 101:1060–1065.

Khalil, B.E., Ibrahim, H.F. & Abd El-Aziz, N.M. (2022). Improvement of *Pichia kudriavzevii* Egyptian isolate for keratinase production. *Egyptian Pharmaceutical Journal*, 21(2), 192.

Kim, J.D. (2007). Purification and characterization of a keratinase from a feather degrading fungus, *Aspergillus flavus* strain K-03, *Mycobiolog,y* 35(4), 219-225.

Kulkarni, P. A. & Devarumath, R.M. (2014). In silico 3D-structure prediction of SsMYB2R: a novel MYB transcription factor from Saccharum spontaneum. *Indian Journal of Biotechnology*, 13:437–447.

Kumar, J. & Yadav, R. (2022). Optimization of cultural conditions for keratinase production by *Curvularia lunata* (JK17) using response surface methodology, *Journal of Scientific Research*, 14 (1), 363-374.

Lateef, A., Adelere, I.A. & Gueguim-Kana, E.B. (2015). *Bacillus safensis* LAU 13: a new source of keratinase and its multi-functional biocatalytic applications. *Biotechnology and Biotechnological Equipment*, 29 (1): 54-63.

Liu, B., Zhang, J., Fang, Z., Gu, L., Liao, X., Du, G. & Chen, J. (2013). Enhanced thermostability of keratinase by computational design and empirical mutation. *Journal of Industrial Microbiology and Biotechnology*, 40:697–704.

Magda, M.A., & Sanaa, T. (2018). High keratinase production and keratin degradation by a mutant strain KR II derived from *Streptomyces radiopugnans* KR 12. *Journal of Applied Biological Sciences*, 12 (1): 18-25.

Marcos, E., Chidyausiku, T. M., McShan, A. C., Evangelidis, T., Nerli, S., Carter, L., Nivón, L. G., Davis, A., Oberdorfer, G., Tripsianes, K., Sgourakis, N. G. & Baker, D. (2018). De novo design of a non-local beta- sheet protein with high stability and accuracy. *Nature Structural and Molecular Biology*, 25(11), 1028–1034.

Mohammadi, A. & Bahramikia, S. (2019). Molecular identification and genetic variation of Alternaria species isolated from tomatoes using ITS1 sequencing and inter simple sequence repeat methods. *Current Medical Mycology*, 5(2), 1.

Moridshahi, R., Bahreini, M., Sharifmoghaddam, M. & Asoodeh, A. (2020). Biochemical characterization of an alkaline surfactant-stable keratinase from a new keratinase producer, *Bacillus zhangzhouensis*. *Extremophiles*, 24(5) :693–704.

Nahar, M.d., Shishir, A., Waliullah, S., Haque, S., Ilias, M., Karim, M.M., Khan, N.S. & Hoq, M. (2016). Cloning, expression, and structure simulation of keratinase from *Bacillus licheniformis* strain

MZK05. *Malaysian Journal of Microbiology*, 12(2):182-190.

Patni, K., Agarwal, P., Kumar, A. & Meena, L.S. (2021). Computational evaluation of anticipated PE_PGRS39 protein involvement in host-pathogen interplay and its integration into vaccine development., *3 Biotech*, 11:204,1-17.

Peng, Z., Mao, X., Zhang, J., Du, G. & Chen, J. (2020). Biotransformation of keratin waste to amino acids and active peptides based on cell-free catalysis., *Biotechnology for biofuels*, 13(1), pp.1-12.

Peng, Z., Zhang, J., Song, Y., Guo, R., Du, G. & Chen, J. (2021). Engineered pro-peptide enhances the catalytic activity of keratinase to improve the conversion ability of feather waste., *Biotechnology and Bioengineering*, 118(7), pp.2559-2571.

Rahimnahal, S., Meimandipour, A., Fayazi, J., Asghar Karkhane, A., Shamsara, M., Beigi Nassiri, M., Mirzaei, H., Hamblin, M.R., Tarrahimofrad, H., Bakherad, H., Zamani, J. & Mohammadi, Y. (2023). Biochemical and molecular characterization of novel keratinolytic protease from *Bacillus licheniformis* (KRLr1). *Frontiers in Microbiology*, 14:1132760.

Reddy, C.C., Khilji, I.A., Gupta, A., Bhuyar, P., Mahmood, S., AL-Japairai, K.A.S., & Chua, G.K. (2021). Valorization of keratin waste biomass and its potential applications. *Journal of Water Process Engineering*, 40, 101707.

Ribeiro, O., Magalhães, F., Aguiar, T.Q., Wiebe, M.G., Penttilä, M. & Domingues, L. (2013). Random and direct mutagenesis to enhance protein secretion in *Ashbyagossypii*, *Bioengineered*, 4(5), 322–331.

Roy, A., Yang, J. & Zhang, Y. (2012). COFACTOR: an accurate comparative algorithm for structure-based protein function annotation. *Nucleic Acids Research*, 40:471–477.

Rozewicki, J., Li, S., Amada, K.M., Standley, D.M., & Katoh, K. (2019). MAFFT-DASH: integrated protein sequence and structural alignment. *Nucleic Acids Research*, 47(W1), W5-W10.

Sahi, S., Tewatia, P. & Malik, B.K. (2012). Modeling, and simulation studies of human b3 adrenergic receptor and its interactions with agonists. *Current Computer-Aided Drug Design*, 8:283–295.

Salim, R.G., Aly, S.E.S., Abo-Sereh, N.A., Hathout, A.S. & Sabry, B.A. (2019). Molecular Identification and Inter-Simple Sequence Repeat (ISSR) Differentiation of Toxigenic *Aspergillus* Strains. *Jordan Journal of Biological Sciences* 12(5).

Saxena, R. & Singh, R. (2010). Statistical optimization of conditions for protease production from *Bacillus sp*. Acta. *Biologica. Szegediensis*. 54(2): 135-141.

Senthivelan, T., Kanagaraja, J., Panda, R.C. & Narayani, T. (2019). Screening, and production of a potential extracellular fungal laccase from *Penicillium chrysogenum*: media optimization by response surface methodology (RSM) and central composite rotatable design (CCRD). *Biotechnology Reports*, 23: e00344.

Siddique, A.M., Nabila, T.N., Ayub, N., Babar, M.E., Rana, S.M., & Rajoka, M.I. (2011). Gamma radiation induced mutagenesis in *Aspergillus niger* to enhance its microbial fermentation activity for

industrial enzyme production, *Molecular Biology Reports*, 38:1367–1374.

Singh, K.D. & Muthusamy, K. (2013). Molecular modeling, quantum polarized ligand docking and structure-based 3D-QSAR analysis of the imidazole series as dual AT1 and ETA receptor antagonists. *Acta Pharmacologica Sinica*, 34:1592–1606.

Suaad, S., Alwakeel., Fuad Ameen., Hussah Al Gwaiz., Hana Sonbol., Salma Alghamdi., Ahmad M Moharram. & Osama Al-Bedak. (2021). Keratinases Produced by *Aspergillus stelliformis*, *Aspergillus sydowii*, and *Fusarium brachygibbosum* Isolated from Human Hair: Yield and Activity. *Journal of Fungi*, 7, 471, 1:13.

Tiwary, E. & Gupta, R. (2010). Medium optimization for a novel 58 kDa dimeric keratinase from *Bacillus licheniformis* ER-15: biochemical characterization and application in feather degradation and dehairing of hides. *Bioresource Technology*, 101(15), 6103-6110.

Vidmar, B. & Vodovnik, M. (2018). Microbial keratinases: Enzymes with promising biotechnological applications. *Food Technology and Biotechnology*, 56 :312–328

Wang, L., Zhou, Y., Huang, Y., Wei, Q., Huang, H. & Guo, C. (2019). Cloning, and expression of a thermostable keratinase gene from *Thermoactinomyces* sp. YT06 in *Escherichia coli* and characterization of purified recombinant enzymes. *World Journal of Microbiology and Biotechnology*, 35(9), 135.

Waterhouse, A., Bertoni, M., Bienert, S., Studer, G., Tauriello, G., Gumienny, R., Heer, F. T., de Beer, T. A. P., Rempfer, C., Bordoli, L., Lepore, R. & Schwede, T. (2018). SWISS-MODEL: Homology modelling of protein structures and complexes., *Nucleic Acids Research*, 46(W1), 296–303.

White, T.J., Bruns, T., Lee, S.J., & Taylor, J. (1990). Amplification, and direct sequencing of fungal ribosomal RNA genes for phylogenetics in: Innis MA, Gelfand DH, Sninsky JJ, White TJ, editors. PCR protocols: a guide to methods and applications. *PCR protocols: a guide to methods and applications,* 18:315-22.

Xin, Z. (2012). Applying the mutation of *Bacillus subtilis* and the optimization of feather fermentation medium to improve Keratinase activity. *A.B.C,* 2(1):64-69.

Xu, D. & Yang, Z. (2013). Ab Initio structure prediction for *Escherichia coli*: towards genome-wide protein structure modeling and fold assignment. *Scientific Reports,* 3(1): 1895.

Yang, J. & Yang, Z. (2015). I-TASSER server: new development for protein structure and function predictions. *Nucleic Acids Research*, 43: W174–W181.

Zhang, Y. (2008). I-TASSER server for protein 3D structure prediction. *BMC Bioinformatics*, 9:1–8

Zheng, W., Zhang, C., Li, Y., Pearce, R., Bell, E.W. & Zhang, Y. (2021). Folding non- homology proteins by coupling deep-learning contact maps with I-TASSER assembly simulations. *Cell Reports Methods*, 1: 100014

Zietkiewicz, E., Rafalski, A. & Labuda, D. (1994). Genome fingerprinting by simple sequence repeat (SSR)-anchored polymerase chain reaction amplification. *Genomics*, 20(2) :176-183.